Available online at www.sciencedirect.com
SCIENCE DIRECT®
Journal of Computational Physics 200 (2004) 718–748
JOURNAL OF COMPUTATIONAL PHYSICS
www.elsevier.com/locate/jcp

A fluid-mixture type algorithm for barotropic two-fluid flow problems

Keh-Ming Shyue

Department of Mathematics, National Taiwan University, Taipei 106 Taiwan, ROC

Received 28 January 2004; received in revised form 28 April 2004; accepted 5 May 2004
Available online 20 July 2004

Abstract

Our goal is to present a simple interface-capturing approach for barotropic two-fluid flow problems in more than one space dimension. We use the compressible Euler equations in isentropic form as a model system with the thermodynamic property of each fluid component characterized by the Tait equation of state. The algorithm uses a non-isentropic form of the Tait equation of state as a basis to the modeling of the numerically induced mixing between two different barotropic fluid components within a grid cell. Similar to our previous work for multicomponent problems, see [J. Comput. Phys. 171 (2001) 678] and references cited therein, we introduce a mixture type of the model system that consists of the full Euler equations for the basic conserved variables and an additional set of evolution equations for the problem-dependent material quantities and also the approximate location of the interfaces. A standard high-resolution method based on a wave-propagation formulation is employed to solve the proposed model system with the dimensional-splitting technique incorporated in the method for multidimensional problems. Several numerical results are presented in one, two, and three space dimensions that show the feasibility of the method as applied to a reasonable class of practical problems without introducing any spurious oscillations in the pressure near the smeared material interfaces.

AMS: 65M06; 76L05; 76M20; 76T05

Keywords: Barotropic flow; Tait equation of state; Stiffened gas equation of state; Fluid-mixture model; Wave propagation method

1. Introduction

In this paper, we are concerned with a model barotropic two-fluid flow problem where the flow regime of interest is assumed to be homogeneous with no jumps in the pressure and velocity (the normal component of it) across a material interface in an $N_d \geqslant 1$ spatial domain. In the problem formulation, we use the isentropic version of the compressible Euler equations of the form

E-mail addresses: shyue@math.ntu.edu.tw, shyue@jacobi.math.ntu.edu.tw (K.-M. Shyue).

0021-9991/$ - see front matter
doi:10.1016/j.jcp.2004.05.003

$$\frac{\partial}{\partial t}\begin{pmatrix}\rho\\ \rho u_i\end{pmatrix}+\sum_{j=1}^{N_d}\frac{\partial}{\partial x_j}\begin{pmatrix}\rho u_j\\ \rho u_i u_j+p(\rho)\delta_{ij}\end{pmatrix}=0 \qquad \text{for } i=1,2,\ldots N_d \tag{1}$$

for the basic equations of motion of each fluid component, where ρ, u_j, p, and δ_{ij} denote the density, the particle velocity in the x_j-direction, the pressure, and the Kronecker delta function, respectively (cf. [9]). To complete the model, the constitutive law for the thermodynamic property of the fluid is taken to satisfy the Tait equation of state for compressible liquids (or called the Murnaghan equation of state in the context of an elastic solid [34]),

$$p(\rho)=(p_0+\mathscr{B})\left(\frac{\rho}{\rho_0}\right)^{\gamma}-\mathscr{B}. \tag{2}$$

Here p_0 and ρ_0 are the reference pressure and density, respectively, $\mathscr{B}$ is a pressure-like constant, and γ is a dimensionless parameter, see [31] for a typical set of material-dependent quantities of practical importance. Representative applications of this two-fluid model are, for instance, to the simulation of the propagation of shock waves in a water–human tissue media in Extracorporeal Shock Wave Lithotripsy [35], or in a water–silicone oil media in the semiconductor industry [57].

To solve this barotropic flow problem numerically, we want to use a generalization of the classical shock-capturing method designed originally for single component flows. For non-barotropic multicomponent problems, it is known in the literature that the principal difficulty in the usual extension is the occurrence of spurious pressure oscillations when two or more fluid components are present in a uniform Cartesian grid cell, see the sample numerical methods proposed in [1–3,12,15,18,21,30,43] for more exposition. For the current application of barotropic flows, there is, however, a relatively few methods developed for the matter, see the recent work of Koren et al. [23], and van Brummelen and Koren [54] for a concise survey.

The approach we take here is to first introduce a non-isentropic form of the Tait equation of state as a basis to the modeling of the mixing between two different barotropic fluid components. Then with the help of a volume-fraction function, we define a hybrid equation of state so that the pressure of the fluid can be determined explicitly no matter what fluid component (pure or not) is within a grid cell (see Section 2). Having that, as in the previous work [45–48], we are able to derive a mixture type of the model system that consists of the full Euler equations for the basic conserved variables and an additional set of evolution equations for the problem-dependent material quantities and also the approximate location of the interfaces. In our approach, the latter equations are included in the algorithm primarily for an easy computation of the pressure from the equation of state, and are put in a form so as to ensure a consistent modeling of the energy equation near the smeared interfaces, and also the fulfillment of the mass equation in the other single component regions. A standard high-resolution method based on a wave-propagation formulation is employed to solve the proposed model system with the dimensional-splitting technique incorporated in the method for multidimensional problems. Numerical results to be presented in Section 6 show that this is a viable approach to a reasonable class of practical problems without producing any wrong oscillations in the pressure near the interfaces.

It should be emphasized that the approach we have proposed here is by no means limited to the two-fluid flows with a Tait equation of state. Extension of the algorithm to other barotropic flow problems with the more general pressure law as occurred in cases with some solid materials (cf. [32,33]), for example, and also to problems involving more than two-flow components, can be made in a similar manner by following the idea described in this paper. Without going into the details for that here, we want to focus our attention to the establishment of the basic solution strategy and validate its use via numerical experimentation of some sample problems.

This paper is organized as follows. In Section 2, we propose a new equation of state for the modeling of the mixing between two different barotropic flows within a grid cell. In Section 3, we describe the model equations that is easy to use for numerical approximation of barotropic two-fluid problems. The construction of the approximate solution for the one-dimensional Riemann problem of the model is discussed in Section 4, and a brief review of numerical methods based on wave propagation is given in Section 5. In Section 6, we present a sample test of results for problems in one, two, and three space dimensions.

2. Equations of state

One of the key elements in our fluid-mixture approach for multicomponent problems is the introduction of a hybrid version of the equation of state that is necessary in the algorithm for modeling the numerical mixing between two different fluid components within a grid cell. In the current instance of barotropic flows, the basic idea of the proposed method is simple. We view the mixture of two different barotropic fluids, where each of them is described by the same Tait equation of state (2) but possibly with a different set of material-dependent quantities: γ, $\mathscr{B}$, and ρ_0, as a non-barotropic fluid, and use an entropy-dependent equation of state for describing the thermodynamic behavior of the fluid mixture instead. By using the first and second laws of thermodynamics (cf. [13,59]) together with (2), it is easy to derive such an equation of state for the pressure p in terms of the mixture density ρ and the specific entropy S as:

$$p(\rho, S) = \mathscr{A}(S)(p_0 + \mathscr{B})\left(\frac{\rho}{\rho_0}\right)^{\gamma} - \mathscr{B}, \tag{3}$$

where $\mathscr{A}(S) = \exp[(S - S_0)/C_V]$ and C_V denotes the specific heat at constant volume. Clearly, (3) reduces to the barotropic flow case (2), when the change of the entropy $\Delta S = S - S_0 \to 0$. In the non-limiting case, however, when ΔS is not close to zero, (3) does give a way to the representation of the cases in between, that is to the mixing of two different barotropic fluids. Numerical experiences indicate that when ΔS is not large, i.e., entropy variation of the fluids is somewhat small, (3) is a good model to use for a reasonable class of practical problems, see Section 6.

It is worthwhile to mention that when we rewrite (3) in terms of the often-used variables in gas dynamics, ρ and the internal energy e, it takes the form

$$p(\rho, e) = (\gamma - 1)\rho\left(e + \frac{\mathscr{B}}{\rho_0}\right) - \gamma\mathscr{B} \tag{4}$$

and when we rewrite (3) in terms of ρ and the temperature T, it becomes

$$p(\rho, T) = \rho RT - \mathscr{B},$$

where R is the universal gas constant. Note that in the fluid dynamical literature an equation of state of the form (4) is typically called the stiffened gas or Tammann equation of state (cf. [14,17]). It is also easy to show that the internal energy of the purely barotropic fluid can be computed by (4) but with the use of (2) directly for the pressure term.

For convenience in the later development, we use a volume-fraction function Y to indicate the type of fluid component within a grid cell (this is a standard way to do in many two-phase flow solver [42,56,58]). For instance, when grid cells contain only fluid-component 1 we may set $Y = 1$, and so when grid cells contain only fluid-component 2 we set $Y = 0$. In case there are some cells cut by the interfaces where $Y \in (0, 1)$, we then have both the fluid-components 1 and 2 occupied by the volume fractions Y and $1 - Y$, respectively. With this definition of Y, the pressure of a barotropic two-fluid flow problem in all the fluid-component scenarios within a grid cell can be determined straightforwardly by:

$$p = \begin{cases} (p_{01} + \mathscr{B}_1)\left(\frac{\rho}{\rho_{01}}\right)^{\gamma_1} - \mathscr{B}_1 & \text{if } Y = 1 \text{ (barotropic fluid 1)}, \\ (p_{02} + \mathscr{B}_2)\left(\frac{\rho}{\rho_{02}}\right)^{\gamma_2} - \mathscr{B}_2 & \text{if } Y = 0 \text{ (barotropic fluid 2)}, \\ (\gamma - 1)\rho\left(e + \frac{\mathscr{B}}{\rho_0}\right) - \gamma\mathscr{B} & \text{if } Y \in (0,1) \text{ (mixture of two barotropic fluids)} \end{cases} \tag{5}$$

provided that all the variables appeared there are defined and known a priori.

Finally, it should be remarked that, in this work, the thermodynamical description of the materials of interest is limited by the stability requirement that the speed of sound of the fluid belongs to a set of real numbers. Certainly, it is both interesting and important to include the cavitation and phase-transition effects to the present constitutive model in a region where the pressure drops to a critical value, but this subject matter is a very difficult one, and is beyond the scope of this paper, see [4,5,11,44,55] and references cited therein for some possible models and approaches proposed in the literature.

3. Equations of motion

We now discuss the model equations that will be used in our numerical methods for constructing approximate solutions of barotropic two-fluid problems. To begin, clearly, in regions where $Y = 0$ or $Y = 1$, it is enough to use (1) and (2) for the complete description of the behavior of the underlying single-component barotropic flow. In regions where $Y \in (0,1)$, however, since the mixture of two barotropic fluid components is modeled in a non-isentropic manner, see Section 2, the original isentropic Eq. (1) are not sufficient to this instance, and so some supplementary equations need to be considered to provide further information of the fluid mixture.

It is apparent that, because the thermodynamic behavior of the fluid mixture depends on the entropy as we have postulated, the conservation law for the total energy of the form

$$\frac{\partial}{\partial t}(\rho E) + \sum_{j=1}^{N_d} \frac{\partial}{\partial x_j}\left(\rho E u_j + p u_j\right) = 0 \tag{6}$$

should be incorporated in the model system, where $E = e + \sum_{j=1}^{N_d} u_j^2/2$ is the specific total energy. In addition to that, as in our previous work on numerical methods for compressible multicomponent problems (cf. [45,46,48]), we also introduce a set of effective equations for the problem-dependent material quantities so that the pressure can be computed easily from the equation of state.

3.1. γ-based effective equations

To derive the aforementioned effective equations for the mixture of material quantities in the present stiffened gas case, it is usual to start with an interface-only problem where both the pressure and each component of the particle velocities are constant in the domain, while the other variables such as the density and the material quantities are having jumps across some interfaces. In this instance, from (1) and (6), it is easy to obtain equations for the time-dependent behavior of the density and total internal energy as

$$\frac{\partial \rho}{\partial t} + \sum_{j=1}^{N_d} u_j \frac{\partial \rho}{\partial x_j} = 0,$$

$$\frac{\partial}{\partial t}(\rho e) + \sum_{j=1}^{N_d} u_j \frac{\partial}{\partial x_j}(\rho e) = 0,$$

in a respective manner. By inserting the equation of state (4) into the latter one, we find an alternative description of the energy equation

$$\frac{\partial}{\partial t}\left(\frac{p+\gamma\mathscr{B}}{\gamma-1}-\frac{\mathscr{B}}{\rho_0}\rho\right)+\sum_{j=1}^{N_d}u_j\frac{\partial}{\partial x_j}\left(\frac{p+\gamma\mathscr{B}}{\gamma-1}-\frac{\mathscr{B}}{\rho_0}\rho\right)=0 \tag{7}$$

that is in relation to not only the pressure, but also the material quantities: γ, $\mathscr{B}$, and ρ_0.

In our algorithm, to maintain the pressure in equilibrium as it should be for our model interface-only problem, we split (7) into the following two equations for the fluid mixtures of $1/(\gamma-1)$ and $\gamma\mathscr{B}/(\gamma-1)-\mathscr{B}\rho/\rho_0$ as

$$\frac{\partial}{\partial t}\left(\frac{1}{\gamma-1}\right)+\sum_{j=1}^{N_d}u_j\frac{\partial}{\partial x_j}\left(\frac{1}{\gamma-1}\right)=0, \tag{8a}$$

$$\frac{\partial}{\partial t}\left(\frac{\gamma\mathscr{B}}{\gamma-1}-\frac{\mathscr{B}}{\rho_0}\rho\right)+\sum_{j=1}^{N_d}u_j\frac{\partial}{\partial x_j}\left(\frac{\gamma\mathscr{B}}{\gamma-1}-\frac{\mathscr{B}}{\rho_0}\rho\right)=0, \tag{8b}$$

respectively. We emphasize that in order to have the correct pressure equilibrium in (7), these are the two key equations that should be satisfied and approximated consistently (when the problem is solved numerically, see Section 5). On the other hand, as a practical matter, it is obvious that, in addition to (8a) and (8b), we need to impose one more additional condition so as to have enough equations for the three material quantities: γ, $\mathscr{B}$, and ρ_0. In our approach (cf. [46,48]), this is done by simply splitting (8b) into the following two parts:

$$\frac{\partial}{\partial t}\left(\frac{\gamma\mathscr{B}}{\gamma-1}\right)+\sum_{j=1}^{N_d}u_j\frac{\partial}{\partial x_j}\left(\frac{\gamma\mathscr{B}}{\gamma-1}\right)=0, \tag{8c}$$

$$\frac{\partial}{\partial t}\left(\frac{\mathscr{B}}{\rho_0}\rho\right)+\sum_{j=1}^{N_d}u_j\frac{\partial}{\partial x_j}\left(\frac{\mathscr{B}}{\rho_0}\rho\right)=0. \tag{8d}$$

Having done so, we arrive at a system of three equations. (8a), (8c), and (8d) for the variables $1/(\gamma-1)$, $\gamma\mathscr{B}/(\gamma-1)$, and $\mathscr{B}\rho/\rho_0$, respectively. Combining them to (1) and (6) yields a model system that is fundamental in our algorithm for describing the behavior of the numerical mixing between two barotropic fluids near the interface. With that, there is no difficulty to compute the pressure from (4) as

$$p=\left[\rho E-\frac{\sum_{j=1}^{N_d}(\rho u_j)^2}{2\rho}+\frac{\mathscr{B}}{\rho_0}\rho-\frac{\gamma\mathscr{B}}{\gamma-1}\right]\Bigg/\left(\frac{1}{\gamma-1}\right).$$

Up to this point, our discussion stresses only on an approach that is capable of keeping the pressure in equilibrium for a model interface-only problem. Since in practice we are interested in shock wave problems as well, we should take the equations, i.e., (8a), (8c), and (8d), in a form such that γ, $\mathscr{B}$, and ρ_0 remain unchanged across both shocks and rarefaction waves. In this regard, it is easy to see that with γ and $\mathscr{B}$ governed by (8a) and (8c), respectively, there is no problem to do so (cf. [1,45]). For ρ_0 or $\mathscr{B}/\rho_0$, however, due to the appearance of the density term in (8d), it turns out that, in a time when such a situation occurs, for consistent with the mass conservation law of the fluid mixture the primitive form of (8d) should be modified by

$$\frac{\partial}{\partial t}\left(\frac{\mathscr{B}}{\rho_0}\rho\right)+\sum_{j=1}^{N_d}\frac{\partial}{\partial x_j}\left(\frac{\mathscr{B}}{\rho_0}\rho u_j\right)=0, \tag{8e}$$

so that the mass-conserving property of the solution in the single component region can be acquired also (cf. [46]). We note that, for convenience, we call the set of equations (8a), (8c), and (8e), a γ-based effective

equations for the mixture of the material quantities of the stiffened gas equation of state to be distinct from the other one presented below.

3.2. Y-based effective equations

Before proceeding further, we note that to find the initial fluid mixtures, $1/(\gamma-1)$, $\gamma\mathscr{B}/(\gamma-1)$, and $\mathscr{B}\rho/\rho_0$, that is necessary when we initialize the data for multicomponent flow computations, we use the equation of state (4), where written as a function of the volume fraction Y_ι, for $\iota = 1, 2$, and $Y_1 + Y_2 = 1$, it reads

$$\frac{p+\gamma\mathscr{B}}{\gamma-1} - \frac{\mathscr{B}}{\rho_0}\rho = \rho e = \sum_{\iota=1}^{2} Y_\iota \rho_\iota e_\iota = \sum_{\iota=1}^{2} Y_\iota \left(\frac{p_\iota + \gamma_\iota \mathscr{B}_\iota}{\gamma_\iota - 1} - \frac{\mathscr{B}_\iota}{\rho_{0\iota}}\rho_\iota \right). \tag{9a}$$

Here the subscript "ι" denotes the state variable of fluid component ι. By taking a similar approach as employed in Section 3.1 for the derivation of the γ-based effective equation (cf. [45,46] also), it comes out easily a splitting of (9a) into the following set of relations:

$$\frac{1}{\gamma-1} = \sum_{\iota=1}^{2} \frac{Y_\iota}{\gamma_\iota - 1}, \qquad \frac{\gamma\mathscr{B}}{\gamma-1} = \sum_{\iota=1}^{2} Y_\iota \frac{\gamma_\iota \mathscr{B}_\iota}{\gamma_\iota - 1}, \quad \text{and} \quad \frac{\mathscr{B}}{\rho_0}\rho = \sum_{\iota=1}^{2} Y_\iota \frac{\mathscr{B}_\iota}{\rho_{0\iota}}\rho_\iota, \tag{9b}$$

where in the process of splitting the terms the pressure p is chosen to satisfy the relation as

$$\frac{p}{\gamma-1} = \sum_{\iota=1}^{2} Y_\iota \frac{p_\iota}{\gamma_\iota - 1}. \tag{9c}$$

With the first part of (9b), it is easy to see that when each of the partial pressures is in equilibrium within a grid cell, the pressure obtained from (9c) would remain in equilibrium also, i.e., $p = p_\iota$, for $\iota = 1, 2$, see [37] for a different way to derive the same result.

Now with the volume-fraction notion of the states $1/(\gamma-1)$, $\gamma\mathscr{B}/(\gamma-1)$, and $\mathscr{B}\rho/\rho_0$ being defined by (9b), the γ-based effective equations may be rewritten into the form:

$$\frac{\partial}{\partial t}\left(\sum_{\iota=1}^{2} \frac{Y_\iota}{\gamma_\iota - 1} \right) + \sum_{j=1}^{N_d} u_j \frac{\partial}{\partial x_j}\left(\sum_{\iota=1}^{2} \frac{Y_\iota}{\gamma_\iota - 1} \right) = 0, \tag{10a}$$

$$\frac{\partial}{\partial t}\left(\sum_{\iota=1}^{2} Y_\iota \frac{\gamma_\iota \mathscr{B}_\iota}{\gamma_\iota - 1} \right) + \sum_{j=1}^{N_d} u_j \frac{\partial}{\partial x_j}\left(\sum_{\iota=1}^{2} Y_\iota \frac{\gamma_\iota \mathscr{B}_\iota}{\gamma_\iota - 1} \right) = 0, \tag{10b}$$

$$\frac{\partial}{\partial t}\left(\sum_{\iota=1}^{2} Y_\iota \frac{\mathscr{B}_\iota}{\rho_{0\iota}}\rho_\iota \right) + \sum_{j=1}^{N_d} \frac{\partial}{\partial x_j}\left(\sum_{\iota=1}^{2} Y_\iota \frac{\mathscr{B}_\iota}{\rho_{0\iota}}\rho_\iota u_j \right) = 0. \tag{10c}$$

After some simple algebraic manipulations (cf. [45]), from both (10a) and (10b), we find the transport equation for each volume fraction Y_ι as

$$\frac{\partial Y_\iota}{\partial t} + \sum_{j=1}^{N_d} u_j \frac{\partial Y_\iota}{\partial x_j} = 0, \tag{10d}$$

while from (10c) we find the mass conservation equation for each fluid component ι as

$$\frac{\partial}{\partial t}(Y_\iota \rho_\iota) + \sum_{j=1}^{N_d} \frac{\partial}{\partial x_j}(Y_\iota \rho_\iota u_j) = 0, \tag{10e}$$

for $\iota = 1, 2$. Clearly, when the set of Y_ι and $Y_\iota\rho_\iota$ are known from (10d) and (10e), we may therefore compute $1/(\gamma-1)$, $\gamma\mathscr{B}/(\gamma-1)$, and $\mathscr{B}\rho/\rho_0$ directly from (9b). Thus, instead of using the γ-based effective equations, it is a viable approach to use the Y-based equations (10d) and (10e), for the motion of the mixture of the material quantities of the problem.

3.3. Complete model system

Note that to constitute a complete model system that is capable of dealing with all the fluid phase cases, $Y = 0$, $Y = 1$, or $Y \in (0, 1)$, we have to know the approximate location of the interfaces so that the correct equations of motion as well as the equation of state can be employed to each part of the domain, from the current time to the next. Here, since $Y_1 + Y_2 = 1$, it is clear that if we choose $Y_1 = Y$ and so $Y_2 = 1 - Y$, the two transport equations in (10d) for each of Y_1 and Y_2 can be combined, without affecting anything, to a single one for Y as

$$\frac{\partial Y}{\partial t} + \sum_{j=1}^{N_d} u_j \frac{\partial Y}{\partial x_j} = 0, \tag{10f}$$

leading to the evolution equation we use in practice for that matter. It is important to mention that, in devising a fluid-mixture type algorithm for multicomponent problems, one common practice (cf. [45,46,48]) is to consider the mixture of the total density, $\rho = Y_1\rho_1 + Y_2\rho_2$, as one of the basic variables, but is not to use the mixtures of the separate fluid densities, $Y_1\rho_1$ and $Y_2\rho_2$, as the basic variables, in the proposed model system. When this is the case, it should be more sensible to use (8e) as the governing equation for the time-evolution of the variable $\mathscr{B}\rho/\rho_0$ than the use of the last relation in (9b) together with one of the equations in (10e) for the determination of $\mathscr{B}\rho/\rho_0$.

Putting all the things together, with the hybrid equation of state (5), the model equations with which we propose to solve the barotropic two-fluid flow problems in more than one space dimension take the form:

$$\begin{aligned}
&\frac{\partial \rho}{\partial t} + \sum_{j=1}^{N_d} \frac{\partial}{\partial x_j}(\rho u_j) = 0,\\
&\frac{\partial}{\partial t}(\rho u_i) + \sum_{j=1}^{N_d} \frac{\partial}{\partial x_j}(\rho u_i u_j + p\delta_{ij}) = 0 \qquad \text{for} \quad i = 1, 2, \ldots, N_d,\\
&\frac{\partial}{\partial t}(\rho E) + \sum_{j=1}^{N_d} \frac{\partial}{\partial x_j}\left(\rho E u_j + p u_j\right) = 0 \qquad \text{if } Y \in (0,1),\\
&\frac{\partial}{\partial t}\left(\frac{\mathscr{B}}{\rho_0}\rho\right) + \sum_{j=1}^{N_d} \frac{\partial}{\partial x_j}\left(\frac{\mathscr{B}}{\rho_0}\rho u_j\right) = 0 \qquad \text{if } Y \in (0,1),\\
&\frac{\partial Y}{\partial t} + \sum_{j=1}^{N_d} u_j \frac{\partial Y}{\partial x_j} = 0.
\end{aligned} \tag{11}$$

Notice that when $Y \in (0, 1)$ we have a system of $N_d + 4$ equations for the motion of the mixing between two barotropic phases. Clearly, the first $N_d + 2$ of them are simply the basic conservation of the mass, momenta (N_d of them), and total energy, while the last two equations are (8e) and (10f) that are introduced to model the fluid-mixing of $\mathscr{B}\rho/\rho_0$ and the volume-fraction function Y (a quantity that is used in the model to identify the approximate location of the interface and also to find γ and $\mathscr{B}$ according to the first two relations in (9b)). On the other instance, when $Y = 0$ or $Y = 1$, we just have the first $N_d + 1$ equations

governing the single-component barotropic flow as usual. With a system expressing in this way, there is no problem to compute all the state variables of interest, including the pressure from the equation of state. The initialization of the state variables in (11) for fluid-mixture cells can be made in a standard way as described in [45,46] for numerical simulations.

Note that, as before, the proposed model system (11) is not written in the full conservation form, but is rather a quasi-conservative system of equations. However, for any given N_d, if the state variables of the flow are all in the region of the thermodynamic stability (this is the case we are interested in here), it is not difficult to show that (11) is a hyperbolic system in the sense that any linear combination of the matrices A_j, $j = 1, 2, \ldots, N_d$, appearing in the quasi-linear form of the equations

$$\frac{\partial q}{\partial t} + \sum_{j=1}^{N_d} A_j(q) \frac{\partial q}{\partial x_j} = 0 \tag{12a}$$

has real eigenvalues and a complete set of eigenvectors.

As an example, we consider the three-dimensional case $N_d = 3$ and then have the state vector q in (12a) defined by

$$q = \left(\rho, \rho u_1, \rho u_2, \rho u_3, \rho E, \frac{\mathscr{B}}{\rho_0}\rho, Y\right)^{\mathrm{T}}, \tag{12b}$$

and the matrices A_j, for $j = 1, 2, 3$, defined by

$$A_1 = \begin{bmatrix} 0 & 1 & 0 & 0 & 0 & 0 & 0 \\ K - u_1^2 & u_1(2-\Gamma) & -u_2\Gamma & -u_3\Gamma & \Gamma & -\Gamma & \chi \\ -u_1u_2 & u_2 & u_1 & 0 & 0 & 0 & 0 \\ -u_1u_3 & u_3 & 0 & u_1 & 0 & 0 & 0 \\ u_1(K-H) & H - u_1^2\Gamma & -u_1u_2\Gamma & -u_1u_3\Gamma & u_1(\Gamma+1) & -u_1\Gamma & u_1\chi \\ -u_1\mathscr{B}/\rho_0 & \mathscr{B}/\rho_0 & 0 & 0 & 0 & u_1 & 0 \\ 0 & 0 & 0 & 0 & 0 & 0 & u_1 \end{bmatrix},$$

$$A_2 = \begin{bmatrix} 0 & 0 & 1 & 0 & 0 & 0 & 0 \\ -u_1u_2 & u_2 & u_1 & 0 & 0 & 0 & 0 \\ K - u_2^2 & -u_1\Gamma & u_2(2-\Gamma) & -u_3\Gamma & \Gamma & -\Gamma & \chi \\ -u_2u_3 & 0 & u_3 & u_2 & 0 & 0 & 0 \\ u_2(K-H) & -u_1u_2\Gamma & H - u_2^2\Gamma & -u_2u_3\Gamma & u_2(\Gamma+1) & -u_2\Gamma & u_2\chi \\ -u_2\mathscr{B}/\rho_0 & 0 & \mathscr{B}/\rho_0 & 0 & 0 & u_2 & 0 \\ 0 & 0 & 0 & 0 & 0 & 0 & u_2 \end{bmatrix},$$

$$A_3 = \begin{bmatrix} 0 & 0 & 0 & 1 & 0 & 0 & 0 \\ -u_1u_3 & u_3 & 0 & u_1 & 0 & 0 & 0 \\ -u_2u_3 & 0 & u_3 & u_2 & 0 & 0 & 0 \\ K - u_3^2 & -u_1\Gamma & -u_2\Gamma & u_3(2-\Gamma) & \Gamma & -\Gamma & \chi \\ u_3(K-H) & -u_1u_3\Gamma & -u_2u_3\Gamma & H - u_3^2\Gamma & u_3(\Gamma+1) & -u_3\Gamma & u_3\chi \\ -u_3\mathscr{B}/\rho_0 & 0 & 0 & \mathscr{B}/\rho_0 & 0 & u_3 & 0 \\ 0 & 0 & 0 & 0 & 0 & 0 & u_3 \end{bmatrix}.$$

With that, the eigenvalues and the corresponding eigenvectors of the matrices are:for matrix A_1,

$$\Lambda_{A_1} = \mathrm{diag}\left(\lambda_1^{(1)}, \lambda_2^{(1)}, \ldots, \lambda_7^{(1)}\right) = \mathrm{diag}(u_1 - c, u_1, u_1 + c, u_1, \ldots, u_1),$$

$$R_{A_1} = \left(r_1^{(1)}, r_2^{(1)}, \ldots, r_7^{(1)}\right) = \begin{bmatrix} 1 & 1 & 1 & 0 & 0 & 0 & 0 \\ u_1 - c & u_1 & u_1 + c & 0 & 0 & 0 & 0 \\ u_2 & u_2 & u_2 & 1 & 0 & 0 & 0 \\ u_3 & u_3 & u_3 & 0 & 1 & 0 & 0 \\ H - u_1 c & K/\Gamma & H + u_1 c & u_2 & u_3 & 1 & -\chi/\Gamma \\ \mathscr{B}/\rho_0 & 0 & \mathscr{B}/\rho_0 & 0 & 0 & 1 & 0 \\ 0 & 0 & 0 & 0 & 0 & 0 & 1 \end{bmatrix},$$

for matrix A_2,

$$\Lambda_{A_2} = \mathrm{diag}\left(\lambda_1^{(2)}, \lambda_2^{(2)}, \ldots, \lambda_7^{(2)}\right) = \mathrm{diag}(u_2 - c, u_2, u_2 + c, u_2, \ldots, u_2),$$

$$R_{A_1} = \left(r_1^{(2)}, r_2^{(2)}, \ldots, r_7^{(2)}\right) = \begin{bmatrix} 1 & 1 & 1 & 0 & 0 & 0 & 0 \\ u_1 & u_1 & u_1 & 1 & 0 & 0 & 0 \\ u_2 - c & u_2 & u_2 + c & 0 & 0 & 0 & 0 \\ u_3 & u_3 & u_3 & 0 & 1 & 0 & 0 \\ H - u_2 c & K/\Gamma & H + u_2 c & u_1 & u_3 & 1 & -\chi/\Gamma \\ \mathscr{B}/\rho_0 & 0 & \mathscr{B}/\rho_0 & 0 & 0 & 1 & 0 \\ 0 & 0 & 0 & 0 & 0 & 0 & 1 \end{bmatrix},$$

and for matrix A_3,

$$\Lambda_{A_3} = \mathrm{diag}\left(\lambda_1^{(3)}, \lambda_2^{(3)}, \ldots, \lambda_7^{(3)}\right) = \mathrm{diag}(u_3 - c, u_3, u_3 + c, u_3, \ldots, u_3),$$

$$R_{A_3} = \left(r_1^{(3)}, r_2^{(3)}, \ldots, r_7^{(3)}\right) = \begin{bmatrix} 1 & 1 & 1 & 0 & 0 & 0 & 0 \\ u_1 & u_1 & u_1 & 1 & 0 & 0 & 0 \\ u_2 & u_2 & u_2 & 0 & 1 & 0 & 0 \\ u_3 - c & u_3 & u_3 + c & 0 & 0 & 0 & 0 \\ H - u_3 c & K/\Gamma & H + u_3 c & u_1 & u_2 & 1 & -\chi/\Gamma \\ \mathscr{B}/\rho_0 & 0 & \mathscr{B}/\rho_0 & 0 & 0 & 1 & 0 \\ 0 & 0 & 0 & 0 & 0 & 0 & 1 \end{bmatrix},$$

$A_j r_k^{(j)} = \lambda_k^{(j)} r_k^{(j)}$, $j = 1, 2, 3$, and $k = 1, 2, \ldots, 7$. Here $c = \sqrt{\gamma(p + \mathscr{B})/\rho}$ is the speed of sound of the fluid, and the other notations appeared in the above formulae are set by $\Gamma = \gamma - 1$, $K = \Gamma \sum_{j=1}^{3} u_j^2/2$, $H = E + p/\rho$, and $\chi = -\Gamma[(p + \gamma_1 \mathscr{B}_1)/(\gamma_1 - 1) - (p + \gamma_2 \mathscr{B}_2)/(\gamma_2 - 1)]$.

For the ease of the latter reference, it is customary to write (11) into a more compact expression by

$$\frac{\partial q}{\partial t} + \sum_{j=1}^{N_d} f_j\left(\frac{\partial}{\partial x_j}, q\right) = 0, \tag{13}$$

where f_j is taken as the vector-value function of the form

$$f_j = \left[\frac{\partial}{\partial x_j}(\rho u_j), \frac{\partial}{\partial x_j}(\rho u_1 u_j + p\delta_{1j}), \ldots, \frac{\partial}{\partial x_j}(\rho u_{N_d} u_j + p\delta_{N_d j}), \frac{\partial}{\partial x_j}(\rho E u_j + p u_j), \frac{\partial}{\partial x_j}\left(\frac{\mathscr{B}}{\rho_0}\rho u_j\right), u_j\frac{\partial Y}{\partial x_j}\right]^T,$$

for $j = 1, 2, \ldots, N_d$. It is easy to see that the functions f_j defined above reduce to the standard flux functions for a single component flow.

To end this section, it is worth mentioning that if for some reasons the variables $Y_1\rho_1$ and $Y_2\rho_2$ are the preferable ones to be used in the algorithm, we may reformulate (11) into an analogous form of the five-equation model advocated by Allaire et al. [3] for compressible multicomponent flow problems. Since this 2-density formulation of the model system will not be considered in the present work, to avoid any possible confusions that may cause, we omit the full description of that model here.

4. Approximate Riemann solvers

Before describing numerical methods to solve (11), we pause to discuss the construction of the Riemann problem solutions in one space dimension which is one of the major steps in our barotropic two-fluid algorithm. If we consider the case $N_d = 3$ as an example, the problem to be solved now is to find the solution of (11) in the direction normal to one of the x_1x_2, x_2x_3, and x_1x_3 planes, with piecewise constant data q_L and q_R to the left and right of the cell interface. It should be noted that in the applications concerned here, we have chosen the data q_L and q_R well enough so that the solution of the Riemann problem would consist of genuinely nonlinear waves such as shock and rarefaction, and linearly degenerate wave such as contact discontinuity; there is no vacuum region occurring in the solution. To simplify the notation in the following discussion, rather than using (u_1, u_2, u_3) for the velocity field as before, we use a simpler version (u, v, w) instead. Without loss of generality, we only look at the Riemann problem in the direction normal to the x_2x_3-plane.

4.1. Shock-only solver

To begin, we are interested in a popular shock-only (or called two-shock) approximation of the Riemann solver that ignores the possibility of rarefaction waves and simply construct a solution in which each pair of the states is connected along the Hugoniot locus for a shock (cf. [7,8]). In this approach, the key step is to find the midstate (u_m, p_m) in the u–p phase plane so that it can connect to (u_L, p_L) by a 1-shock, and to (u_R, p_R) by a 3-shock. It is well known that this is equivalent to solving the following nonlinear equation in an iterative manner for the pressure p_m:

$$h(p_m) = u_{mR}(p_m) - u_{mL}(p_m) = 0. \tag{14}$$

Here u_{mL} and u_{mR} are the velocities defined by connecting the states along the 1-shock and 3-shock curves, respectively,

$$u_{mL}(p) = u_L - \frac{p - p_L}{M_L(p)}, \qquad u_{mR}(p) = u_R + \frac{p - p_R}{M_R(p)}, \tag{15}$$

with M_ι denoting the Lagrangian shock speed, for $\iota = L$ or R. In the current application of the pressure law (5), we may compute M_ι quite easily by evaluating the formula

$$M_\iota^2(p) = \begin{cases} \frac{p - p_\iota}{\rho_\iota^{-1} - \rho_{m\iota}^{-1}(p)} & \text{if } Y = 1 \text{ or } Y = 0 \\ C_\iota^2\left[1 + \left(\frac{\gamma_\iota + 1}{2\gamma_\iota}\right)\left(\frac{p + \mathscr{B}_\iota}{p_\iota + \mathscr{B}_\iota} - 1\right)\right] & \text{if } Y \in (0, 1), \end{cases} \tag{16}$$

where $C_\iota = \rho_\iota c_\iota$ is the Lagrangian sound speed, and $\rho_{m\iota}$ is the midstate density on the ι side,

$$\rho_{m\iota}(p) = \begin{cases} \rho_{0\iota}\left(\frac{p+\mathscr{B}_\iota}{p_{0\iota}+\mathscr{B}_\iota}\right)^{1/\gamma_\iota} & \text{if } Y = 1 \text{ or } Y = 0, \\ \left[\rho_\iota^{-1} - \frac{p-p_\iota}{M_\iota^2(p)}\right]^{-1} & \text{if } Y \in (0,1). \end{cases} \tag{17}$$

Note that (16) and (17) are as a result derived from the Rankine–Hugoniot jump conditions across the shock waves (cf. [9]).

When applying a standard root-finding approach such as the secant method to (14), we have a 2-step iteration scheme as follows:

$$p_{\mathrm{m}}^{(n+1)} = p_{\mathrm{m}}^{(n)} - \frac{\left|p_{\mathrm{m}}^{(n)} - p_{\mathrm{m}}^{(n-1)}\right|}{\left|u_{\mathrm{mL}}^{(n)} - u_{\mathrm{mL}}^{(n-1)}\right| + \left|u_{m\mathrm{R}}^{(n)} - u_{\mathrm{mR}}^{(n-1)}\right|}\left[u_{\mathrm{mR}}^{(n)} - u_{\mathrm{mL}}^{(n)}\right], \tag{18}$$

where $u_{m\iota}^{(n)} = u_{m\iota}[p_{\mathrm{m}}^{(n)}]$, for $\iota = \mathrm{L}$ or R, and $n = 1, 2, \ldots$ (until convergence). With a suitable choice of the starting values $p_{\mathrm{m}}^{(0)}$ and $p_{\mathrm{m}}^{(1)}$, method (18) typically converges to the exact solution p_{m} at a superlinear rate [22]. For gas dynamics, it is a common practice to set $p_{\mathrm{m}}^{(0)}$ and $p_{\mathrm{m}}^{(1)}$ by

$$\begin{aligned} p_{\mathrm{m}}^{(0)} &= \frac{p_{\mathrm{R}}C_{\mathrm{L}} + p_{\mathrm{L}}C_{\mathrm{R}} - (u_{\mathrm{R}} - u_{\mathrm{L}})C_{\mathrm{L}}C_{\mathrm{R}}}{C_{\mathrm{L}} + C_{\mathrm{R}}}, \\ p_{\mathrm{m}}^{(1)} &= \frac{p_{\mathrm{R}}M_{\mathrm{L}}^{(0)} + p_{\mathrm{L}}M_{\mathrm{R}}^{(0)} - (u_{\mathrm{R}} - u_{\mathrm{L}})M_{\mathrm{L}}^{(0)}M_{\mathrm{R}}^{(0)}}{M_{\mathrm{L}}^{(0)} + M_{\mathrm{R}}^{(0)}}, \end{aligned} \tag{19}$$

where $M_\iota^{(0)} = M_\iota[p_{\mathrm{m}}^{(0)}]$. Having that, we may assign $u_{\mathrm{mL}}^{(0)}$ and $u_{\mathrm{mR}}^{(0)}$ by

$$u_{\mathrm{mL}}^{(0)} = u_{\mathrm{L}} - \frac{p_{\mathrm{m}}^{(0)} - p_{\mathrm{L}}}{C_{\mathrm{L}}}, \qquad u_{m\mathrm{R}}^{(0)} = u_{\mathrm{R}} + \frac{p_{\mathrm{m}}^{(0)} - p_{\mathrm{R}}}{C_{\mathrm{R}}},$$

and $u_{\mathrm{mL}}^{(1)}$ and $u_{\mathrm{mR}}^{(1)}$ according to (15). After a satisfactory convergence of the scheme, u_{m} can then be calculated based on the formula:

$$u_{\mathrm{m}} = \frac{p_{\mathrm{L}} - p_{\mathrm{R}} + u_{\mathrm{L}}M_{\mathrm{L}}(p_{\mathrm{m}}) + u_{\mathrm{R}}M_{\mathrm{R}}(p_{\mathrm{m}})}{M_{\mathrm{L}}(p_{\mathrm{m}}) + M_{\mathrm{R}}(p_{\mathrm{m}})}.$$

We note that alternatively we may use a 1-step Newton method for the solution of (14). In this case, the iteration scheme reads as follows:

$$p_{\mathrm{m}}^{(n+1)} = p_{\mathrm{m}}^{(n)} - \frac{Z_{\mathrm{L}}^{(n)}Z_{\mathrm{R}}^{(n)}}{Z_{\mathrm{L}}^{(n)} + Z_{\mathrm{R}}^{(n)}}\left[u_{\mathrm{mR}}^{(n)} - u_{\mathrm{mL}}^{(n)}\right], \tag{20}$$

where $Z_\iota^{(n)} = Z_\iota[p_{\mathrm{m}}^{(n)}]$, for $\iota = \mathrm{L}$ or R, and $n = 1, 2, \ldots$ (until convergence). Again with (5) it is an easy matter to evaluate Z_ι by

$$Z_\iota^2(p) = \left|\frac{\mathrm{d}p_{\mathrm{m}}}{\mathrm{d}u_{\mathrm{m}}}\right| = \begin{cases} \frac{2C_{m\iota}^2(p)}{M_\iota^2 + C_{m\iota}^2(p)}M_\iota & \text{if } Y = 1 \text{ or } Y = 0, \\ \frac{2M_\iota^2}{M_\iota^2 + C_\iota^2}M_\iota & \text{if } Y \in (0,1), \end{cases} \tag{21}$$

where $C_{m\iota} = \rho_{m\iota}c_{m\iota}$. Here the initial guess of the iteration $p_{\mathrm{m}}^{(0)}$ can be taken in the same way as in (19) for the secant method. It is known that the rate of convergence of method (20) is quadratic, when $p_{\mathrm{m}}^{(0)}$ is sufficiently close to p_{m} (cf. [22]).

Fig. 1 shows a typical solution structure of the two-fluid Riemann problem considered here. Clearly, in a shock-only approximate solver, we replace the leftward-going rarefaction wave by a 1-shock and so the solution consists of three discontinuities moving at constant speeds. Here the propagation speed of each discontinuity is determined by

$$\lambda_1 = u_{\mathrm{m}} - \frac{M_{\mathrm{L}}(p_{\mathrm{m}})}{\rho_{\mathrm{mL}}(p_{\mathrm{m}})}, \qquad \lambda_2 = u_{\mathrm{m}}, \qquad \lambda_3 = u_{\mathrm{m}} + \frac{M_{\mathrm{R}}(p_{\mathrm{m}})}{\rho_{\mathrm{mR}}(p_{\mathrm{m}})}, \tag{22}$$

with the jumps across each of them computed by the difference between the states to the left and right of the discontinuity,

$$\mathscr{W}_1 = q_{\mathrm{mL}} - q_{\mathrm{L}}, \qquad \mathscr{W}_2 = q_{\mathrm{mR}} - q_{\mathrm{mL}}, \qquad \mathscr{W}_3 = q_{\mathrm{R}} - q_{\mathrm{mR}}, \tag{23}$$

where $q_{m\iota}$ is calculated from (12b) using the data: $\rho_{m\iota}$, u_{m}, p_{m}, v_ι, w_ι, $\mathscr{B}_\iota$, $\rho_{0\iota}$, $p_{0\iota}$, and Y_ι, for $\iota = \mathrm{L}$ or R. As usual, wave propagation methods (to be described in Section 5) are based on using these propagating discontinuities to update the cell averages in the cells neighboring each interface.

4.2. HLL-type solver

We are next concerned with a simple variant of the Riemann solver based on the work of Harten et al. [16] for general hyperbolic systems of conservation laws,

$$\frac{\partial q}{\partial t} + \frac{\partial}{\partial x} f(q) = 0, \tag{24}$$

where $q \in \mathbb{R}^n$ is the vector of conserved variables for a system of n equations, and f is the flux function. Recall that in the original version of the HLL solver, the solution of the Riemann problem is assumed to be composed of two discontinuities propagating at constant speeds λ_{L} and λ_{R} to the left and right, separating three constant states in the x–t space. If we assume further that λ_{L} and λ_{R} are known a priori by some simple estimates based on the local information of the wave speeds (cf. [10,52]), then by using the integral form of the conservation laws over a sufficiently large control volume $[-M, M] \times [0, T]$, for some M and $T \in \mathbb{R}$, it is

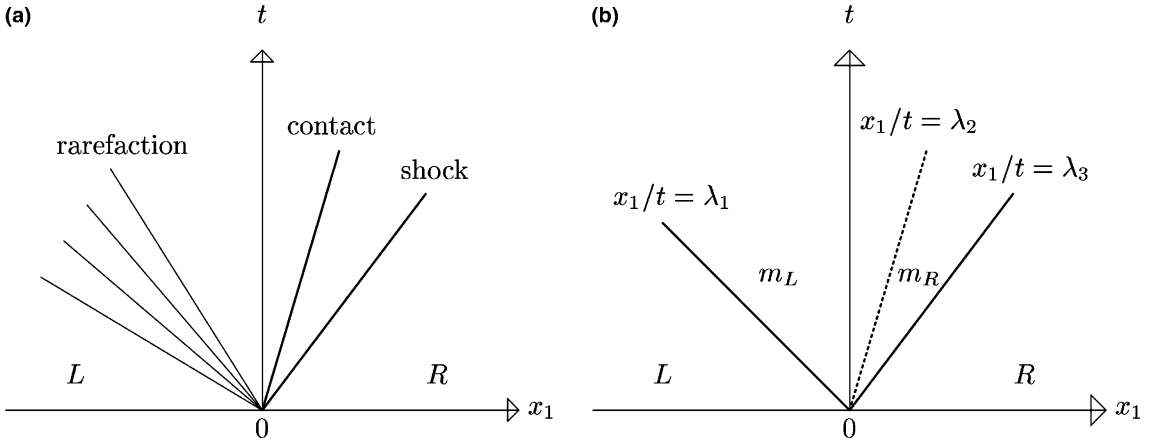

Fig. 1. (a) A typical solution structure of the Riemann problem. (b) Solution structure of the shock-only and HLLC approximate Riemann solvers. Note that in the original HLL solver the wave family associated with λ_2 is not present in the solution.

an easy matter to find the constant state in the middle region, denoted by q_{m}, as the average of the exact solution over the interval $[T\lambda_{\mathrm{L}}, T\lambda_{\mathrm{R}}]$ at time T,

$$q_{\mathrm{m}} = \frac{1}{T(\lambda_{\mathrm{R}} - \lambda_{\mathrm{L}})} \int_{T\lambda_{\mathrm{L}}}^{T\lambda_{\mathrm{R}}} q(x,T)\,\mathrm{d}x = \frac{\lambda_{\mathrm{R}} q_{\mathrm{R}} - \lambda_{\mathrm{L}} q_{\mathrm{L}} - f(q_{\mathrm{R}}) + f(q_{\mathrm{L}})}{\lambda_{\mathrm{R}} - \lambda_{\mathrm{L}}}, \tag{25}$$

where $f(q_\iota)$ is the flux evaluated at the state q_ι, for $\iota = \mathrm{L}$ or R.

While the above 2-wave HLL solver has been used quite successfully in many numerical methods for computing approximate solutions of (24), it is known that the numerical result obtained by using this solver is too diffusive for problems with contact discontinuities (cf. [52]). In addition to that, because of the lack of information on the structure of the interfaces, it is not an adequate approach at all for general multi-component problems.

To improve upon this 2-wave Riemann solver, we take a method suggested by Toro et al. [6,53] in that an additional middle wave of speed u_{m} is included in the solution structure for modeling the speed of contact discontinuity, yielding a 3-wave HLL (or called HLLC) solver. Note that if we have had the first two components of q_{m} computed from (25), we may simply set $u_{\mathrm{m}} = q_{\mathrm{m}}^{(2)}/q_{\mathrm{m}}^{(1)}$, where $q_{\mathrm{m}}^{(i)}$ is the ith component of the vector q_{m}, see [52] for the various other ways to compute u_{m}.

With that, our goal next is to find the constant states q_{mL} and q_{mR} in the regions m_{L} and m_{R} to the left and right of the middle wave, respectively. We do this by using the integral form of the conservation laws again, but now applied over a control volume $[-M, u_{\mathrm{m}}T - \epsilon] \times [0,T]$ for the state q_{mL}, and over a control volume $[u_{\mathrm{m}}T + \epsilon, M] \times [0,T]$ for the state q_{mR}, $0 < \epsilon \ll 1$. When the aforementioned procedure is applied to the current two-fluid model (11), it is not difficult to show that the result is

$$\begin{aligned}
&q_{m\iota}^{(1)} = \frac{f_{m\iota}^{(1)}}{\lambda_\iota - u_{\mathrm{m}}}, \qquad q_{m\iota}^{(2)} = u_{\mathrm{m}} q_{m\iota}^{(1)}, \qquad q_{m\iota}^{(3)} = v_\iota q_{m\iota}^{(1)}, \qquad q_{m\iota}^{(4)} = w_\iota q_{m\iota}^{(1)},\\
&q_{m\iota}^{(5)} = \frac{f_{m\iota}^{(5)} + u_{\mathrm{m}}\left(u_{\mathrm{m}} f_{m\iota}^{(1)} - f_{m\iota}^{(2)}\right)}{\lambda_\iota - u_{\mathrm{m}}}, \qquad q_{m\iota}^{(6)} = \frac{f_{m\iota}^{(6)}}{\lambda_\iota - u_{\mathrm{m}}}, \qquad q_{m\iota}^{(7)} = q_\iota^{(7)},
\end{aligned} \tag{26}$$

where $f_{m\iota}^{(i)} = \lambda_\iota q_\iota^{(i)} - f^{(i)}(q_\iota)$ represents the ith component of the vector $f_{m\iota}$, for $\iota = \mathrm{L}$ or R. It is easy to check that $q_{\mathrm{mL}}^{(i)}$ and $q_{\mathrm{mR}}^{(i)}$ satisfy the basic consistency condition of the integral form of the conservation laws,

$$\left(\frac{u_{\mathrm{m}} - \lambda_{\mathrm{L}}}{\lambda_{\mathrm{R}} - \lambda_{\mathrm{L}}}\right) q_{\mathrm{mL}}^{(i)} + \left(\frac{\lambda_{\mathrm{R}} - u_{\mathrm{m}}}{\lambda_{\mathrm{R}} - \lambda_{\mathrm{L}}}\right) q_{\mathrm{mR}}^{(i)} = q_{\mathrm{m}}^{(i)},$$

for $i = 1, 2, \ldots, 6$. As in the shock-only solver, we then set the speed of the three moving discontinuities by $\lambda_1 = \lambda_{\mathrm{L}}$, $\lambda_2 = u_{\mathrm{m}}$, $\lambda_3 = \lambda_{\mathrm{R}}$, with the choice of $\lambda_{\mathrm{L}} = \min(u_{\mathrm{L}} - c_{\mathrm{L}}, u_{\mathrm{R}} - c_{\mathrm{R}})$ and $\lambda_{\mathrm{R}} = \max(u_{\mathrm{L}} + c_{\mathrm{L}}, u_{\mathrm{R}} + c_{\mathrm{R}})$ as an example, and the jumps across each of them by (23) using the result (26).

To end this section, it should be mentioned that, when computing the Riemann problem solution of (11), the iterative shock-only solver described in the beginning of this section is a much more expensive method to use as compared to the non-iterative 3-wave HLLC solver. But due to the careful construction of the middle state solution for the contact discontinuity, which is extremely important for many difficult multicomponent problems with strong shock waves and stiff equations of state, we observe typically a better behavior of the results when the shock-only solver is in use than the HLLC solver is in use in a numerical method for approximating solutions of practical problems. Surely, to improve efficiency, one may take a hybrid approach that utilizes the HLLC solver only in case for a single-fluid Riemann problem, but employs the shock-only solver in case for two-fluid Riemann problems otherwise. Finally, we note that it is still unclear on how to define the associated average states in a suitable way that linearizes the matrices in (12a), leading to an efficient and accurate Roe solver for the class of two-fluid Riemann problem considered here.

5. Numerical methods

To find approximate solutions of our model system (11) for barotropic two-fluid problems, we use a high-resolution wave propagation method developed by LeVeque [25,27] for general hyperbolic systems of partial differential equations. This method is a variant of the fluctuation-and-signal scheme of Roe [39,40] in that we solve one-dimensional Riemann problems at each cell interface, and use the resulting waves (i.e., discontinuities moving at constant speeds) to update the solutions in neighboring grid cells. To achieve high resolution (i.e., second-order accurate on smooth solutions, and sharp and monotone profiles on discontinuous solutions), we introduce slopes and limiters to the method as in many other high-resolution schemes for conservation laws [14,26,51]. Here, for simplicity, rather than using x_1, x_2, and x_3 for the spatial variables, we take the often-employed x, y, and z in a respective manner, instead.

5.1. One-dimensional case

We begin our discussion by reviewing the basic idea of the method for solving the simplest $N_d = 1$ case of our model system,

$$\frac{\partial q}{\partial t} + f_1\left(\frac{\partial}{\partial x}, q\right) = 0,$$

with q and f_1 defined as in (13). To discretize the solution state, we take a uniform grid with fixed mesh spacing Δx in the x-direction and use a standard finite-volume formulation in which the value Q_j^n approximates the cell average of the solution over the grid cell $[x_j, x_{j+1}]$ at time t_n,

$$Q_j^n \approx \frac{1}{\Delta x}\int_{x_j}^{x_{j+1}} q(x, t_n)\,\mathrm{d}x.$$

The time step from the current time t_n to the next t_{n+1} is denoted by Δt.

5.1.1. First-order method

In this numerical discretization setup, a first-order accurate version of the method in wave-propagation form is a Godunov-type scheme that can be written as

$$Q_j^{n+1} = Q_j^n - \frac{\Delta t}{\Delta x}\sum_{m=1}^{m_w}\left(\lambda_{\mathrm{m}}^- \mathscr{W}_{\mathrm{m}}\right)_{j+1}^n + \left(\lambda_{\mathrm{m}}^+ \mathscr{W}_{\mathrm{m}}\right)_j^n, \tag{27}$$

where λ_{m} and $\mathscr{W}_{\mathrm{m}}$ are solutions of the mth wave family, for $m = 1, 2, \ldots, m_w$, obtained from solving the Riemann problems at cell interfaces x_j and x_{j+1} with the properly chosen approximate solver as described in Section 4, and $\lambda^- = \min(\lambda, 0)$, $\lambda^+ = \max(\lambda, 0)$. It is known that method (27) belongs to a class of upwind schemes and is stable when the typical CFL (Courant–Friedrichs–Lewy) condition is satisfied (cf. [14,26,28]). Moreover, it is not difficult to show that the method is quasi-conservative in the sense that when applying the method to (11) not only the conservation laws but also the transport equations are approximated in a consistent manner by the method, see [46] for the details.

In devising an efficient solver for multicomponent problems, it is of fundamental importance to look into an interface-only problem (cf. [45,46]) and check to see whether or not an oscillation-free results can be obtained by using the proposed numerical algorithm. Without loss of generality, here we consider a single two-fluid Riemann problem where at cell interface x_j the initial data consists of uniform pressure p_0 and constant velocity u_0 to the left and right of the interface, but having jumps on the other state variables such as ρ, γ, $\mathscr{B}$, ρ_0, and Y. If we now assume a positive velocity $u_0 > 0$, and take a shock-only solver (see Section 4.1) for the Riemann problem solution, from (27) the cell average Q_j^n would be updated by

$$Q_j^{n+1} = Q_j^n - \frac{\Delta t}{\Delta x}(\lambda_2 \mathscr{W}_2)_j^n, \tag{28a}$$

or equivalently by

$$\begin{bmatrix} \rho \\ \rho u \\ \rho E \\ \mathscr{B}\rho/\rho_0 \\ Y \end{bmatrix}_j^{n+1} = \begin{bmatrix} \rho \\ \rho u_0 \\ \rho E \\ \mathscr{B}\rho/\rho_0 \\ Y \end{bmatrix}_j^n - \frac{\Delta t}{\Delta x} u_0 \begin{bmatrix} \Delta\rho \\ u_0\Delta\rho \\ \Delta(\rho E) \\ \Delta(\mathscr{B}\rho/\rho_0) \\ \Delta Y \end{bmatrix}_j^n, \tag{28b}$$

when expressing (28a) in terms of the solution states of the problem. Noting that in this case the difference operator Δ is simply applied to the Riemann data Q_{j-1}^n and Q_j^n on the left and right of the interface.

If we substitute the first equation of (28b) into the second one, it follows quite easily that we have the expected quantity of the particle velocity $u_j^{n+1} = u_0$. With this result, the third equation of (28b) can be simplified to

$$(\rho e)_j^{n+1} = (\rho e)_j^n - \frac{\Delta t}{\Delta x} u_0 \Delta(\rho e)_j^n$$

or alternatively to

$$\left(\frac{p+\gamma\mathscr{B}}{\gamma-1} - \frac{\mathscr{B}}{\rho_0}\rho\right)_j^{n+1} = \left(\frac{p+\gamma\mathscr{B}}{\gamma-1} - \frac{\mathscr{B}}{\rho_0}\rho\right)_j^n - \frac{\Delta t}{\Delta x} u_0 \Delta\left(\frac{p+\gamma\mathscr{B}}{\gamma-1} - \frac{\mathscr{B}}{\rho_0}\rho\right)_j^n,$$

when employing the equation of state of the form (4). It is important to note that, when the fluid is barotropic, the total internal energy of the flow can be calculated directly by using (4) together with (2) for the pressure term. Thus we may use it to define the total energy for purely barotropic flows as in the case for the non-barotropic flows (i.e., the mixture of two different barotropic fluid components), yielding the viability of the above formula, no matter what type of the fluid component is present in the Riemann data.

If we proceed our computation by applying the fourth equation of (28b) to the above equation, we obtain further simplification

$$\left(\frac{p+\gamma\mathscr{B}}{\gamma-1}\right)_j^{n+1} = \left(\frac{p+\gamma\mathscr{B}}{\gamma-1}\right)_j^n - \frac{\Delta t}{\Delta x} u_0 \Delta\left(\frac{p+\gamma\mathscr{B}}{\gamma-1}\right)_j^n.$$

Now the replacement of γ and $\mathscr{B}$ by the volume-fraction relations in (9b) would lead to an alternative form of the above equation as

$$\left(\sum_{\imath=1}^{2} Y_\imath \frac{p+\gamma_\imath\mathscr{B}_\imath}{\gamma_\imath-1}\right)_j^{n+1} = \left(\sum_{\imath=1}^{2} \frac{p_0+\gamma_\imath\mathscr{B}_\imath}{\gamma_\imath-1}(Y_\imath)_j^n\right) - \frac{\Delta t}{\Delta x} u_0 \left(\sum_{\imath=1}^{2} \frac{p_0+\gamma_\imath\mathscr{B}_\imath}{\gamma_\imath-1}(\Delta Y_\imath)_j^n\right).$$

Then, after a simple manipulation, we get the desired pressure equilibrium $p_j^{n+1} = p_0$, under the condition of the fulfillment of the difference equations for the volume fraction $Y_\imath$,

$$(Y_\imath)_j^{n+1} = (Y_\imath)_j^n - \frac{\Delta t}{\Delta x} u_0 \Delta(Y_\imath)_j^n$$

for $\imath = 1, 2$. Note that this is exactly the last equation of (28b), because we have employed the notations in which $Y_1 = Y$ and $Y_2 = 1 - Y$.

Having shown this, it is also easy to demonstrate that, if the HLLC solver (see Section 4.2) is used instead for solving the aforementioned interface-only problem, we get the same Riemann problem solution as presented in (28b), and hence obtain the same numerical result of the problem.

5.1.2. High-resolution method

To improve the accuracy of method (27) to second-order, it is a customary approach by first introducing correction waves in a piecewise-linear form with zero mean value and then propagating each wave over the time step Δt to update the cell averages it overlaps. Without providing the details here (cf. [28,29] for example), with the corrections, (27) is modified by

$$Q_j^{n+1} := Q_j^{n+1} - \frac{\Delta t}{2\Delta x}\sum_{m=1}^{m_w}\left[|\lambda_m|\left(1-|\lambda_m|\frac{\Delta t}{\Delta x}\right)\widetilde{\mathscr{W}}_m\right]_{j+1}^{n} - \left[|\lambda_{\mathrm{m}}|\left(1-|\lambda_m|\frac{\Delta t}{\Delta x}\right)\widetilde{\mathscr{W}}_{\mathrm{m}}\right]_j^{n}, \tag{29}$$

where $\widetilde{\mathscr{W}}_m$ is a limited value of $\mathscr{W}_{\mathrm{m}}$ obtained by comparing $\mathscr{W}_m$ with the corresponding $\mathscr{W}_m$ from the neighboring Riemann problem to the left (if $\lambda_m > 0$) or to the right (if $\lambda_m < 0$).

Note that with the use of the wave-form representation of the Riemann solver as described in Section 4, it is quite common to perform the limiting procedure over each component of the wave via a limiter function Φ (e.g., by using the minmod function $\Phi(\theta) = \max(0, \min(1, \theta))$ or some others as discussed in [51]), and set

$$\widetilde{\mathscr{W}}_{mj}^{(i)} = \Phi\left(\theta_{mj}^{(i)}\right)\mathscr{W}_{mj}^{(i)} \quad \text{with} \quad \theta_{mj}^{(i)} = \frac{\mathscr{W}_{mJ}^{(i)}}{\mathscr{W}_{mj}^{(i)}}, \qquad J = \begin{cases} j-1 & \text{if } \lambda_{mj} \geqslant 0, \\ j+1 & \text{if } \lambda_{mj} < 0, \end{cases} \tag{30}$$

where $\mathscr{W}_{mj}^{(i)}$ is the ith component of $\mathscr{W}_{mj}$. While this approach works in a satisfactory manner without causing any wrong oscillations for the 1- and 3-waves, it was mentioned in [46,48] that, for the 2-wave, the third limited component on the total energy $\widetilde{\mathscr{W}}_{2j}^{(3)}$ should be modified to ensure a consistent approximation of that term, yielding the desired pressure equilibrium near the interfaces.

To demonstrate how the modification needs to be done in the current barotropic flow model (11), we use the interface-only problem described in Section 5.1.1 as an example. Then from (29) the cell average Q_j^{n+1} obtained using (28a) would be updated by

$$Q_j^{n+1} := Q_j^{n+1} - \frac{\Delta t}{2\Delta x}|\lambda_2|\left(1-|\lambda_2|\frac{\Delta t}{\Delta x}\right)\left(\widetilde{\mathscr{W}}_{2,j+1} - \widetilde{\mathscr{W}}_{2j}\right)^n, \tag{31a}$$

or equivalently by

$$\begin{bmatrix} \rho \\ \rho u \\ \rho E \\ \mathscr{B}\rho/\rho_0 \\ Y \end{bmatrix}_j^{n+1} := \begin{bmatrix} \rho \\ \rho u \\ \rho E \\ \mathscr{B}\rho/\rho_0 \\ Y \end{bmatrix}_j^{n+1} - \frac{\mu}{2}(1-\mu)\begin{bmatrix} \Phi\left[(\Delta\rho)_j/(\Delta\rho)_{j+1}\right](\Delta\rho)_{j+1} \\ u_0\Phi\left[(\Delta\rho)_j/(\Delta\rho)_{j+1}\right](\Delta\rho)_{j+1} \\ \Phi\left[(\Delta\rho E)_j/(\Delta\rho E)_{j+1}\right](\Delta\rho E)_{j+1} \\ \Phi\left[(\Delta\mathscr{B}\rho/\rho_0)_j/(\Delta\mathscr{B}\rho/\rho_0)_{j+1}\right](\Delta\mathscr{B}\rho/\rho_0)_{j+1} \\ \Phi\left[(\Delta Y)_j/(\Delta Y)_{j+1}\right](\Delta Y)_{j+1} \end{bmatrix}^n$$

$$+\frac{\mu}{2}(1-\mu)\begin{bmatrix} \Phi\left[(\Delta\rho)_{j-1}/(\Delta\rho)_j\right](\Delta\rho)_j \\ u_0\Phi\left[(\Delta\rho)_{j-1}/(\Delta\rho)_j\right](\Delta\rho)_j \\ \Phi\left[(\Delta\rho E)_{j-1}/(\Delta\rho E)_j\right](\Delta\rho E)_j \\ \Phi\left[(\Delta\mathscr{B}\rho/\rho_0)_{j-1}/(\Delta\mathscr{B}\rho/\rho_0)_j\right](\Delta\mathscr{B}\rho/\rho_0)_j \\ \Phi\left[(\Delta Y)_{j-1}/(\Delta Y)_j\right](\Delta Y)_j \end{bmatrix}^n, \tag{31b}$$

when applying the limiter function (30) to the above equation, and letting $\mu = u_0\Delta t/\Delta x$. Note that, from the first two equations of (31b), we find easily $u_j^{n+1} = u_0$ that is independent of the limiter being employed to the method. Clearly, as in the first-order case, to maintain the pressure in equilibrium, the results that are used for the solutions of $\mathscr{B}\rho/\rho_0$ and Y in the fourth and fifth components of (31b), respectively, should be incorporated into the computation of the total energy, i.e., in the third component of (31b). But the definition of $\widetilde{\mathscr{W}}_{2j}^{(3)}$ employed in (31b) does not respect this fact, in general, for any chosen limiter function, and so it should not be the correct form to be used in practice for this matter.

Motivated by the previous work (cf. [46,48]), one possible approach is to make a new definition of $\widetilde{\mathscr{W}}_{2j}^{(3)}$ as

$$\widetilde{\mathscr{W}}_{2j}^{(3)} := \Phi\left[\frac{(\Delta\kappa)_{j-1}}{(\Delta\kappa)_j}\right](\Delta\kappa)_j + \sum_{\iota=1}^{2}\frac{\gamma_\iota\mathscr{B}_\iota}{\gamma_\iota - 1}\Phi\left[\frac{(\Delta Y_\iota)_{j-1}}{(\Delta Y_\iota)_j}\right](\Delta Y_\iota)_j - \Phi\left[\frac{(\Delta\mathscr{B}\rho/\rho_0)_{j-1}}{(\Delta\mathscr{B}\rho/\rho_0)_j}\right](\Delta\mathscr{B}\rho/\rho_0)_j,$$

where $\kappa = \rho E - \gamma\mathscr{B}/(\gamma-1) + \mathscr{B}\rho/\rho_0$, or alternatively in addition to that one may set the first term on the right-hand side of the expression as

$$\Phi\left[\frac{(\Delta\kappa)_{j-1}}{(\Delta\kappa)_j}\right](\Delta\kappa)_j := \frac{1}{2}u_{*j}^2\Phi\left[\frac{(\Delta\rho)_{j-1}}{(\Delta\rho)_j}\right](\Delta\rho)_j + p_{*j}\sum_{\iota=1}^{2}\frac{1}{\gamma_\iota - 1}\Phi\left[\frac{(\Delta Y_\iota)_{j-1}}{(\Delta Y_\iota)_j}\right](\Delta Y_\iota)_j.$$

Here u_{*j} and p_{*j} are the midstate solutions of the Riemann problem at cell interface x_j. With any of these revisions of the limited 2-wave on the total energy, it is not difficult to show that for the interface-only problem we again have the required pressure equilibrium in the solution of the method. Moreover, we obtain a better resolution of the result as compared to the first-order result, see Fig. 2 for an example.

5.2. Multidimensional case

To extend the one-dimensional wave propagation method to more space dimensions, here we take a simple dimensional-splitting approach in which a multidimensional problem is split into a sequence of one-dimensional problems. Consider the three-dimensional case $N_d = 3$, for example. The barotropic two-fluid flow problem modeled by (13),

$$\frac{\partial q}{\partial t} + f_1\left(\frac{\partial}{\partial x}, q\right) + f_2\left(\frac{\partial}{\partial y}, q\right) + f_3\left(\frac{\partial}{\partial z}, q\right) = 0$$

can be split into

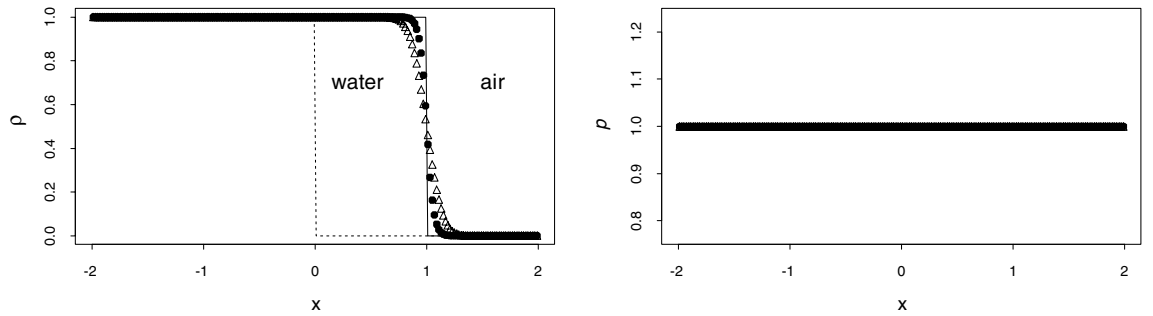

Fig. 2. Numerical results for an interface-only problem at time $t = 0.01$. The triangles shows result obtained using the first-order method, while the filled octagons shows the result using the high-resolution method. The solid line is the exact solution.

$$x\text{-sweeps}: \quad \frac{\partial q}{\partial t} + f_1\left(\frac{\partial}{\partial x}, q\right) = 0, \tag{32a}$$

$$y\text{-sweeps}: \quad \frac{\partial q}{\partial t} + f_2\left(\frac{\partial}{\partial y}, q\right) = 0, \tag{32b}$$

$$z\text{-sweeps}: \quad \frac{\partial q}{\partial t} + f_3\left(\frac{\partial}{\partial z}, q\right) = 0. \tag{32c}$$

Assuming a uniform Cartesian grid with fixed mesh spacing Δx, Δy, and Δz in the x-, y-, and z-direction, respectively. In a finite-volume formulation of the solution, the value Q^n_{ijk} would approximate the cell average of the solution over the (i,j,k)th grid cell at time t_n,

$$Q^n_{ijk} \approx \frac{1}{\Delta x \Delta y \Delta z} \int\int\int_{\mathscr{C}_{ijk}} q(x,y,z,t_n)\,\mathrm{d}x\,\mathrm{d}y\,\mathrm{d}z,$$

where $\mathscr{C}_{ijk} = [x_i, x_{i+1}] \times [y_j, y_{j+1}] \times [z_k, z_{k+1}]$ denotes the cubical region occupied by the grid cell (i,j,k). Then a dimensional-splitting (or called Godunov-splitting) version of the first-order wave propagation method in three dimensions can be written as:

$$Q^*_{ijk} = Q^n_{ijk} - \frac{\Delta t}{\Delta x} \sum_{m=1}^{m_w} \left(\lambda^{(x)-}_m \mathscr{W}^{(x)}_m\right)^n_{i+1,jk} + \left(\lambda^{(x)+}_m \mathscr{W}^{(x)}_m\right)^n_{ijk}, \tag{33a}$$

$$Q^{**}_{ijk} = Q^*_{ijk} - \frac{\Delta t}{\Delta y} \sum_{m=1}^{m_w} \left(\lambda^{(y)-}_m \mathscr{W}^{(y)}_m\right)^*_{i,j+1,k} + \left(\lambda^{(y)+}_m \mathscr{W}^{(y)}_m\right)^*_{ijk}, \tag{33b}$$

$$Q^{n+1}_{ijk} = Q^{**}_{ijk} - \frac{\Delta t}{\Delta z} \sum_{m=1}^{m_w} \left(\lambda^{(z)-}_m \mathscr{W}^{(z)}_m\right)^{**}_{ij,k+1} + \left(\lambda^{(z)+}_m \mathscr{W}^{(z)}_m\right)^{**}_{ijk}. \tag{33c}$$

Note that in the x-sweeps we start with cell average Q^n_{ijk} at time t_n and solve (32a) along each row of cells $\mathscr{C}_{ijk}$ with j and k fixed, updating Q^n_{ijk} to Q^*_{ijk} by the use of (33a), where $\lambda^{(x)}_{m,ijk}$ and $\mathscr{W}^{(x)}_{m,ijk}$ are solutions of the mth wave family obtained from solving the one-dimensional Riemann problems in the direction normal to the cell interface between $\mathscr{C}_{ijk}$ and $\mathscr{C}_{i+1,jk}$ with Q^n_{ijk} and $Q^n_{i+1,jk}$ as initial data. Then in the y-sweeps we can use the Q^*_{ijk} values as data for solving (32b) along each column of cells $\mathscr{C}_{ijk}$ with i and k fixed, which gives us Q^{**}_{ijk} from (33b). Finally, in the z-sweeps we use the Q^{**}_{ijk} values as data for solving (32c) along the other column of cells $\mathscr{C}_{ijk}$ with i and j fixed, yielding the solution of the next time step Q^{n+1}_{ijk} from (33c).

To improve numerical accuracy of this splitting method, in each one-dimensional sweep, we may simply apply the same high-resolution approach as discussed in Section 5.1.2 to the current multidimensional problem. Note that, for an interface-only problem in multiple space dimensions, by performing a similar analysis as done in Section 5.1, it is not difficult to show that the method described above gives the correct pressure equilibrium without introducing any spurious oscillations near the smeared interface, see Fig. 5 for a numerical example in two space dimensions.

It should be mentioned that, except for some simple problems, there will be generally splitting error of the method just described (cf. [28]). But from numerical experiences it turns out that the splitting error is often no worse than the errors introduced by the numerical methods in each sweep, and hence it is typically not necessary to use a more accurate splitting approach such as the Strang splitting [50] to reduce the splitting error, see [28] for some discussion of why one might not want to use a higher order splitting

method. In addition, a sample of three-dimensional computations done by J.O. Langseth for vorticity generated by a shock wave hitting a cylinder of low-density gas even shows good result using the present method as compared to the fully discrete wave propagation method (cf. [24,25,27]), see the CLAWPACK webpage: "http://www.amath.washington.edu/~claw", for the details. For these reasons, we will use the one-dimensional high-resolution wave propagation method together with the Godunov splitting for all the multidimensional tests done in the next section.

6. Numerical results

We now present results to validate our numerical algorithm described in Section 5 for barotropic two-fluid problems. We start our computations by performing a couple of tests in one space dimension and then do some more tests in multiple space dimensions. Without stating otherwise, we run all the problems using the HLLC Riemann solver, the "minmod" limiter in a high-resolution method, and the Courant number $\nu = 0.9$.

6.1. One-dimensional case

Example 6.1.1. To begin with, we consider an interface-only problem of van Brummelen and Koren [54] in which the exact solution of the problem is a single air–water material interface evolving in air with uniform equilibrium pressure $p_0 = 1$ and constant particle velocity $u_0 = 100$. Initially, the interface is located at the center of the computational domain $x \in [-2, 2]$. On the left of the interface, the fluid is a water-like material with

$$(\rho_0, \gamma, \mathscr{B}, Y)_{\mathrm{L}} = (1, 7, 3000, 1),$$

while on the right of the interface, the fluid is an air-like material with

$$(\rho_0, \gamma, \mathscr{B}, Y)_{\mathrm{R}} = \left(10^{-3}, 1.4, 0, 0\right).$$

Note that with the data given above we may determine the density ρ by simply using the Tait equation of state (2).

For this problem, calculations were carried out by using both the first-order and high-resolution version of the method with a 200-cell grid. Snapshots of the density and pressure at time $t = 0.01$ are shown in Fig. 2. It is clear that the pressure obtained using each of these methods remains at the correct constant state p_0 without any spurious oscillations near the numerically diffused air–water interface. Moreover, we get a better result in the density when the high-resolution method is in use in the computation.

Example 6.1.2. Our next example is concerned with a more general data for two-fluid Riemann problem. In this case, in region where $x \in [-2, 0)$, we have an air-like material with the state variables

$$(p, u, \rho_0, \gamma, \mathscr{B}, Y)_{\mathrm{L}} = \left(10^3, 0, 10^{-3}, 1.4, 0, 1\right),$$

while in region where $x \in [0, 2]$, we have a water-like material with the state variables

$$(p, u, \rho_0, \gamma, \mathscr{B}, Y)_{\mathrm{R}} = (1, 0, 1, 7, 3000, 0).$$

Here the reference pressure $p_0 = 1$ is taken throughout the domain. With this initial condition, breaking of the air–water membrane would result in a self-similar solution in the x–t space that consists of a leftward-going rarefaction wave, a rightward-going contact discontinuity, and a shock wave.

Fig. 3 shows high-resolution result for the density, momentum, and pressure, at time $t = 0.01$ using 200 mesh points. From the displayed profiles, we clearly observe the correct behavior and good resolution of the computed contact discontinuity, and also the shock and rarefaction waves as in comparison with the exact solution.

Example 6.1.3. As an example to verify convergence of the computed solutions to the correct weak ones, we consider a shock-contact interaction problem studied by van Brummelen and Koren [54]. In this problem, the initial condition we take is composed of three constant states with data

$$\begin{pmatrix} p \\ u \\ \rho_0 \\ \gamma \\ \mathscr{B} \\ Y \end{pmatrix}_{\mathrm{L}} = \begin{pmatrix} 10^3 \\ 6.3386 \\ 1 \\ 7 \\ 3000 \\ 1 \end{pmatrix}, \quad \begin{pmatrix} p \\ u \\ \rho_0 \\ \gamma \\ \mathscr{B} \\ Y \end{pmatrix}_{\mathrm{M}} = \begin{pmatrix} 1 \\ 0 \\ 1 \\ 7 \\ 3000 \\ 1 \end{pmatrix}, \quad \begin{pmatrix} p \\ u \\ \rho_0 \\ \gamma \\ \mathscr{B} \\ Y \end{pmatrix}_{\mathrm{R}} = \begin{pmatrix} 1 \\ 0 \\ 10^{-3} \\ 1.4 \\ 0 \\ 0 \end{pmatrix},$$

which is the same data as used in [54] with the exception that on the state L a larger magnitude of the pressure and velocity are employed here as opposed to $p_{\mathrm{L}} = 10$ and $u_{\mathrm{L}} = 0.062$. Here L is the state used for $x \in [-2, -0.1)$, M is the state used for $x \in [-0.1, 0)$, and R is the state used for $x \in [0, 2]$. We note that this gives us one example in which a stationary air–water interface is accelerated by a shock wave coming from the heavy-fluid (water) to the light-fluid (air) region. In one dimension, it is known that the resulting solution after the interaction would consist of a transmitted shock wave, an interface, and a reflected rarefaction wave.

Numerical result for a run until time $t = 0.01$ is shown in Fig. 4, where we again solve the problem using the high-resolution method with 200 mesh points, and plot the snapshot of ρ, ρu, and p at the stopping time. We can easily see that the shock wave and contact discontinuity are very well located, and the rarefaction wave moves at the correct speed with the correct shape. A multidimensional version of the problem will be considered in the following section.

6.2. Multidimensional case

Example 6.2.1. We now test our algorithm for a two-dimensional form of the interface-only problem that the solution consists of a circular water column evolving in air with uniform equilibrium pressure and constant particle velocity throughout the domain. As an example, we take the similar set of data as in Example 6.1.1 that initially inside the column of radius $r_0 = 0.16$, we have a water-like material as

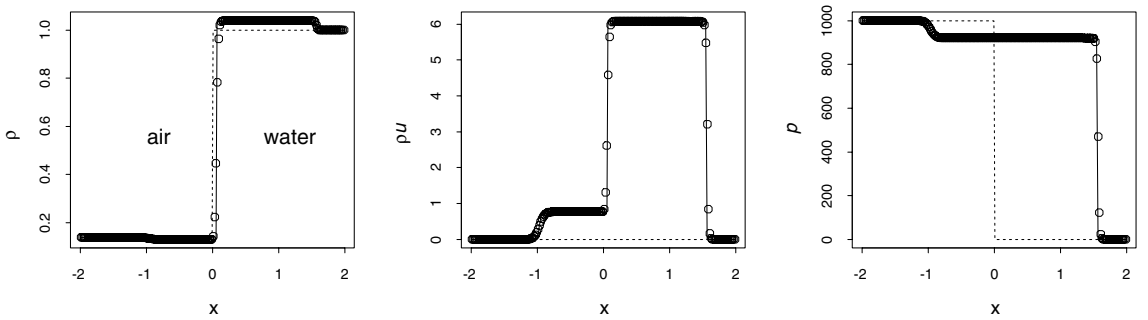

Fig. 3. High-resolution results for a two-fluid Riemann problem at time $t = 0.01$. The solid line is the exact solution and the points shows the computed solution with 200 mesh points. The dashed line in each subplot is the initial condition at time $t = 0$.

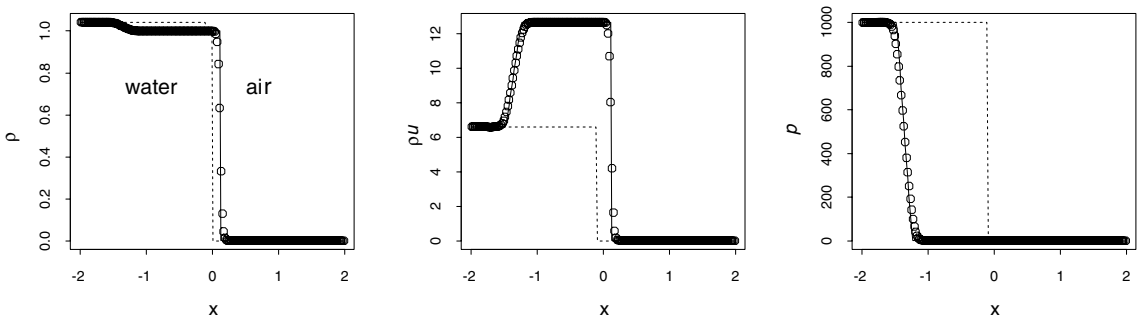

Fig. 4. High-resolution results for a shock-contact interaction problem at time $t = 0.01$. The graphs of the solution are displayed in the same manner as in Fig. 3.

$$(p, u, v, \rho_0, \gamma, \mathscr{B}, Y)_{r \leqslant r_0} = \left(1, 10^2, 10^2, 1, 7, 3000, 1\right),$$

while outside the column we have an air-like material as

$$(p, u, v, \rho_0, \gamma, \mathscr{B}, Y)_{r > r_0} = \left(1, 10^2, 10^2, 10^{-3}, 1.4, 0, 0\right).$$

Here $r = \sqrt{(x - x_0)^2 + (y - y_0)^2}$ is the distance from a point (x, y) in a unit square domain to the center of the water column $(x_0, y_0) = (0.25, 0.25)$.

In Fig. 5, we show results obtained using the high-resolution method with a 100×100 grid, where the 3D surface plots of the density and pressure, and the cross-section plots of the density and pressure along $x = y$ are presented at time $t = 0.005$. From the figure, it is easy to observe good agreement of the numerical solutions as compared with the exact results. Notice in particular that the computed pressure remains in equilibrium as desired, without any spurious oscillations near the smeared air–water column interface.

Example 6.2.2. We next consider a radially symmetric problem so that the computed solutions in two space dimensions can be compared to the one-dimensional results for numerical validation. In this test, we use the following two-phase (air–water) flow data for experiments in which, in the air phase, the state variables are

$$(p, u, v, \rho_0, \gamma, \mathscr{B}, Y) = \begin{cases} (10^3, 0, 0, 10^{-3}, 1.4, 0, 1) & \text{if } r \leqslant r_1 \\ (10^{-3}, 0, 0, 10^{-3}, 1.4, 0, 1) & \text{if } r > r_2, \end{cases}$$

while in the water phase they are

$$(p, u, v, \rho_0, \gamma, \mathscr{B}, Y) = (1, 0, 0, 1, 7, 3000, 0) \qquad \text{if } r_1 < r \leqslant r_2,$$

where $r = \sqrt{x^2 + y^2}$, $r_1 = 0.2$, and $r_2 = 1$. Here due to the pressure difference between the fluids at $r = r_1$, breaking of the inner circular membrane occurs instantaneously, yielding an outward-going shock wave in water, an inward-going rarefaction wave in air, and a contact discontinuity lying in between that separates the air and water. As times go along, the inward-going wave would be reflected from the geometric center that generates a new outward-going wave and induces the subsequent interaction of waves. At a somewhat later time, the outward-going shock wave would be collided with the outer air–water interface at $r = r_2$ that results in a wave pattern consisting of a transmitted shock wave, an interface, and a reflected rarefaction wave. Because of the symmetry of the solution, for simplicity, we only take a quarter of the $[-1.2, 1.2] \times [-1.2, 1.2]$ domain, and apply the line of symmetry boundary conditions to the bottom and the left sides during the computations.

Figs. 6 and 7 show numerical results for the density, radial velocity (defined as $\bar{u} = \sqrt{u^2 + v^2}$), pressure, and volume fraction at three stopping times, $t = 0.0015$, 0.003, and 0.007, where the test has been carried

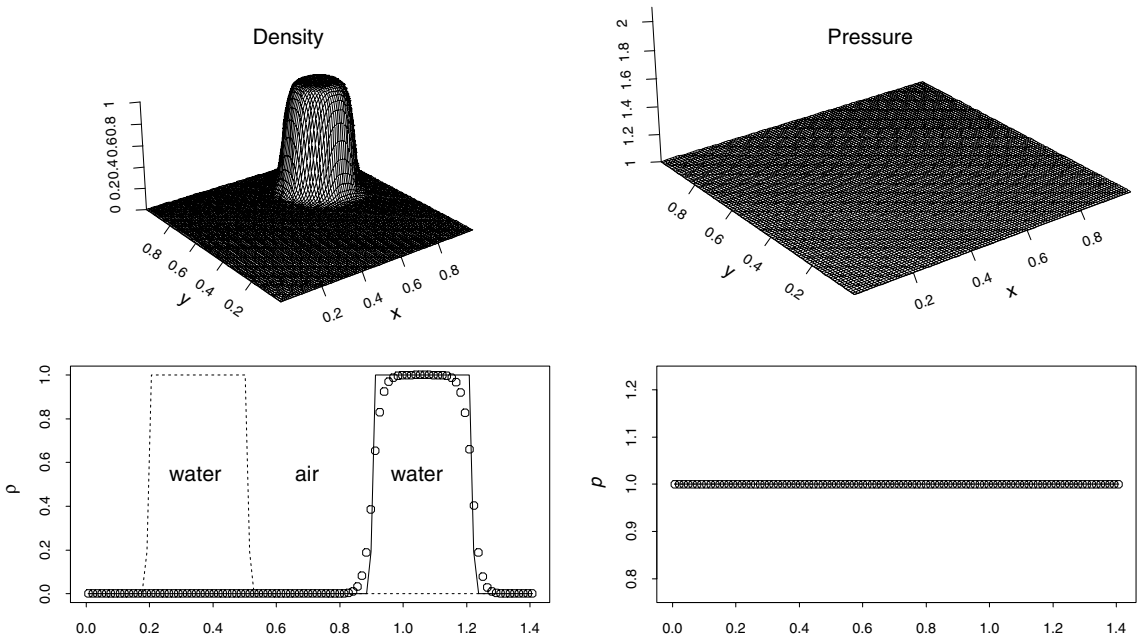

Fig. 5. High-resolution results for a two-dimensional interface-evolving problem at time $t = 0.005$. On the first row: Surface plots of the density and pressure. On the second row: Cross-sectional plots of the density and pressure along line $x = y$. The solid line in the cross-sectional plot is the exact solution, the dotted points are the numerical results, and the dashed line is the initial condition at time $t = 0$.

out by using a 240×240 grid with the high-resolution method. Clearly, from the contour plots shown in Fig. 6, we observe good resolution of the solution structure (i.e., both the shock and interface remain circular and appear to be very well located) after the breaking of the membrane and also the interaction of the shock and the outer interface. Note that, in the contours of pressure at time $t = 0.007$, there are little wiggles near 16° to the x- and y-axis which may be viewed as grid-alignment effects with the use of the high-resolution method. It should be mentioned that this type of error is not present when the problem is solved by using the first-order method (not shown), and is less visible when the problem is solved by using a smaller time step in the high resolution method than the time step taken here with the Courant number $\nu = 0.9$.

The scatter plots shown in Fig. 7 provide the validation of our two-dimensional results as in comparison with the "true" solution obtained from solving the one-dimensional model with appropriate source terms for the radial symmetry, using the high-resolution method with a 1200 mesh points. That is, for the equation, we have a modified-version of the model (13) in one dimension as

$$\frac{\partial q}{\partial t} + f\left(\frac{\partial}{\partial r}, q\right) = \psi(q) \tag{34}$$

with f a vector-value function defined by

$$f = \left[\frac{\partial}{\partial r}(\rho u), \frac{\partial}{\partial r}\left(\rho u^2 + p\right), \frac{\partial}{\partial r}(\rho E u + p u), \frac{\partial}{\partial r}\left(\frac{\mathscr{B}}{\rho_0}\rho u\right), u\frac{\partial Y}{\partial r}\right]^{\mathrm{T}},$$

and ψ the source term derived directly from the geometric simplification of a multidimensional flow to a one-dimensional one,

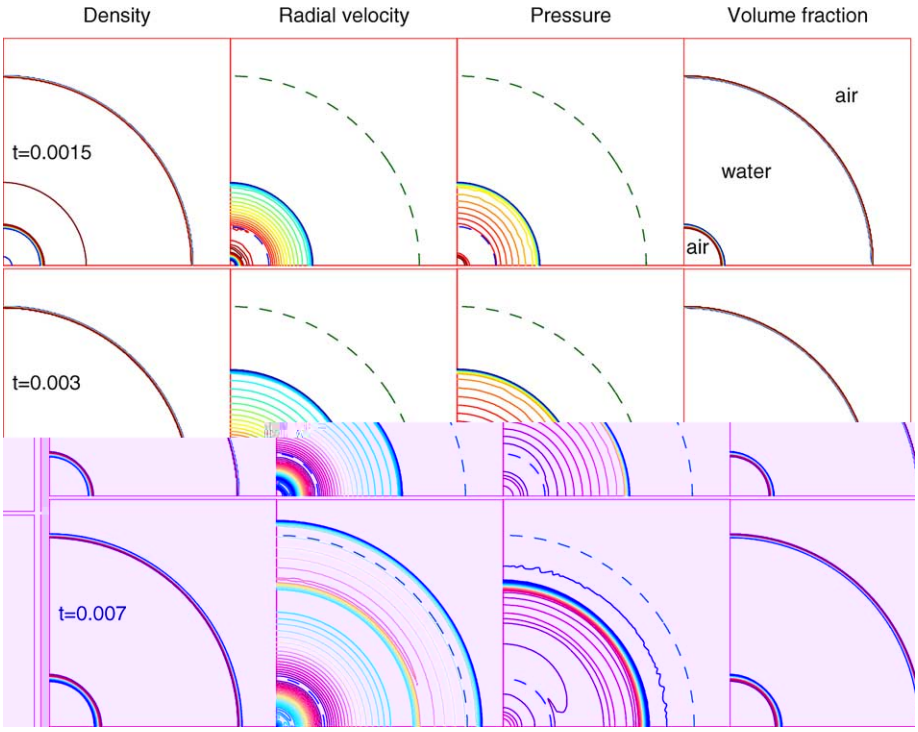

Fig. 6. High-resolution results for a radially symmetric problem. Contour plots for the density, radial velocity, pressure, and volume fraction are shown at three different times $t = 0.0015$, 0.003, and 0.007. The dashed line shown in the graph is the approximate location of the air–water interface.

$$\psi = -\frac{\alpha}{r}\left(\rho u, \rho u^2, \rho E u + p u, \frac{\mathscr{B}}{\rho_0}\rho u, 0\right)^{\mathrm{T}}.$$

Note that in the case of a 2D radially or 3D spherically symmetric flow, we use the quantity $\alpha = 1$ or 2, respectively; u now denotes the particle velocity in the r-(radial) direction. We use a Strang-type time splitting procedure [50] to deal with the geometric sources of (34) in a high-resolution manner during the run. From the figure, it is clear that our results agree quite well with the "true" solutions at all the selected times, and also free of wrong fluctuations in the pressure near the inner and outer interfaces before and after the interactions of rarefaction and shock waves.

Example 6.2.3. To show how our algorithm works on shock waves in a more general two-dimensional geometry, we are concerned with the simulation of a shock wave in liquid over a gas bubble. For this problem, we take a shock tube of size $[0, 2] \times [0, 0.6]$, and consider the initial condition that is composed of a planarly rightward-going shock wave in water traveling at $x = 0.4$ from left to right, and a stationary air bubble of radius $r_0 = 0.2$ located at $(x_0, y_0) = (0.8, 0)$ on the right of the shock wave. Similar to the data employed in Example 6.1.3, inside the air bubble, we have the data

$$(p, u, v, \rho_0, \gamma, \mathscr{B}, Y) = \left(1, 0, 0, 10^{-3}, 1.4, 0, 1\right),$$

while outside the air bubble (the fluid is water), we use the pre-shock state

$$(p, u, v, \rho_0, \gamma, \mathscr{B}, Y) = (1, 0, 0, 1, 7, 3000, 0),$$

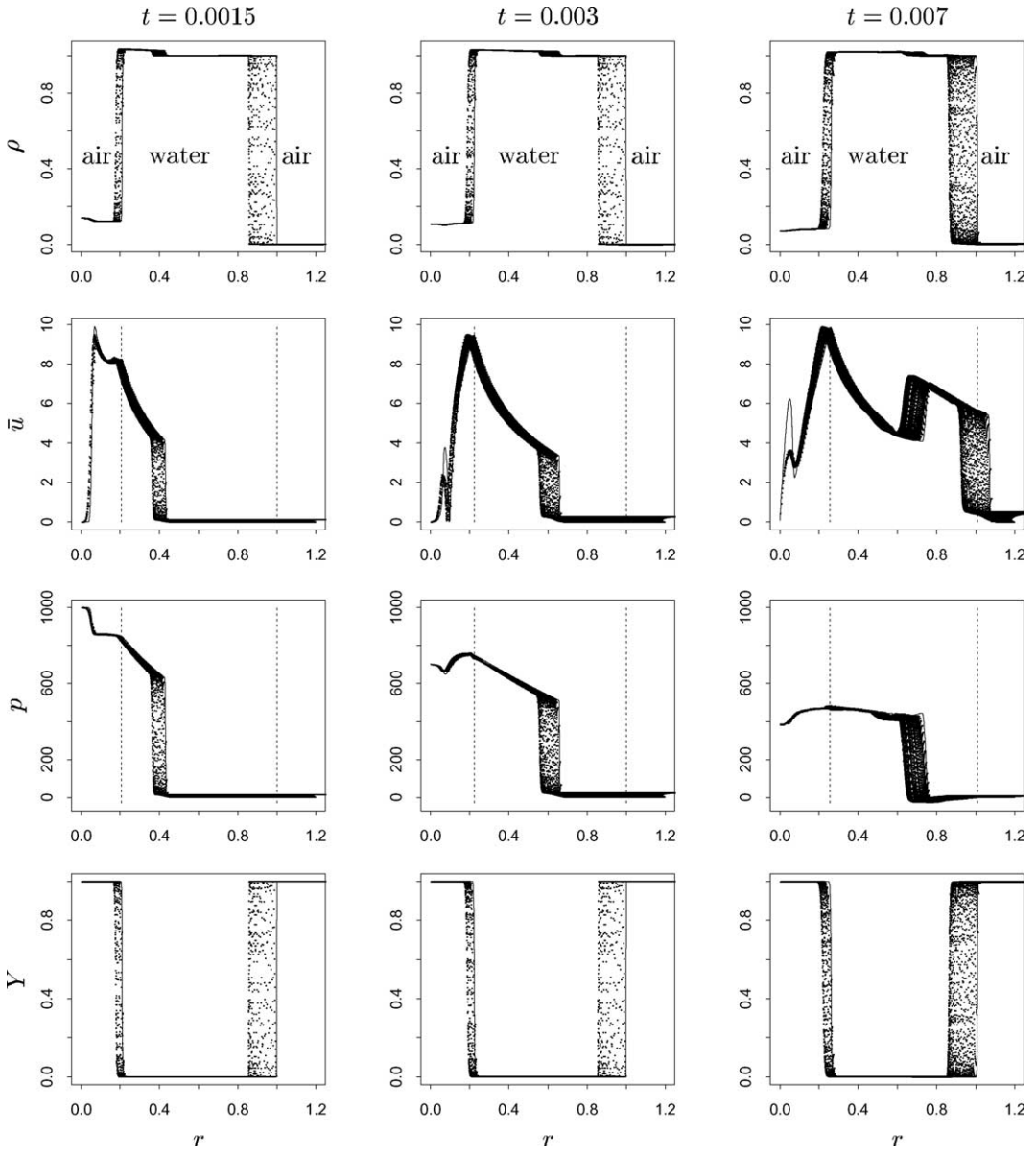

Fig. 7. Scatter plots of the results for the run shown in Fig. 6. The solid line is the "true" solution obtained from solving the one-dimensional model with appropriate source terms for the radial symmetry using the high-resolution method and 1200 mesh points. The dotted points are the two-dimensional result. The dashed line is the approximate location of the air–water interface.

and the post-shock state

$$(p, u, v, \rho_0, \gamma, \mathscr{B}, Y) = \left(10^3, 6.3386, 0, 1, 7, 3000, 0\right).$$

Note that in carrying out the computations below, we have used the non-reflecting boundary condition on the left and right sides, the solid wall boundary condition on the top and bottom sides.

Figs. 8 and 9 show numerical results of a sample run using a 400×120 grid. From Fig. 8, we observe the distortion of the air bubble and the somewhat complicated wave pattern after the passage of the shock wave to the bubble, where a Schlieren-type images of the density, pressure, and volume fraction are presented at four different times $t = i \times 0.0025$, for $i = 1, 2, 3, 4$. The cross section of the results for the same run along the bottom boundary is drawn in Fig. 9, giving some quantitative information about the density, pressure, and volume fraction at the selected times. It is easy to notice that on the fourth snapshot of the pressure, i.e., the plot at the time $t = 0.01$, there is a small portion of the domain in the water phase which contains negative value of the pressure. In the current model with the pressure law (5), this is, however, permitted as long as the pressure stays within the region of the thermodynamic stability of the flow, see Section 2. Note that in that figure we have also included results obtained using the same method but with a finer 800×240 grid, observing good agreement of these two solutions.

To check the correctness of the computed solutions further, we perform a mesh refinement test of the algorithm using a grid sequence: $2^i(200 \times 60)$, for $i = 0, 1, 2$. Numerical results of the y-averaged data, defined as $\bar{\zeta}(x) = \sum_{j=1}^{M} \zeta(x, y_j)/M$, for $\zeta = \rho$, p, or Y, are drawn in Fig. 10 at the snapshot time $t = 0.01$, where M is the total number of grid cells in the y-direction. From the plot, we clearly find a good convergence behavior of the solutions under mesh refinement. To show a temporal resolution of the result, in Fig. 11 we present the circulation of the velocity vector $\vec{V} = (u, v)$ around the closed boundary curve of the domain, noticing basically the same qualitative behavior of the solution as the mesh is refined, see [38] for a similar results of a shock wave in air over an R22 bubble, and [36] for more discussion about the vorticity generation by shock wave propagation through bubbles in gas.

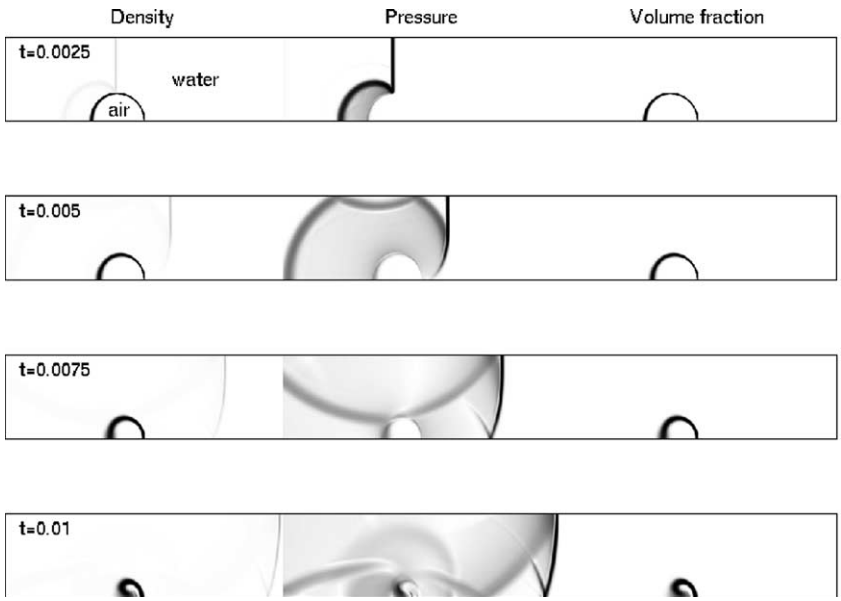

Fig. 8. Two-dimensional results for a planar shock wave in water over an air bubble. Schlieren-type images for the density, pressure, and volume fraction are shown at four different times $t = i \times 0.0025$, for $i = 1, 2, 3, 4$, where a 400×120 grid was used in the computation.

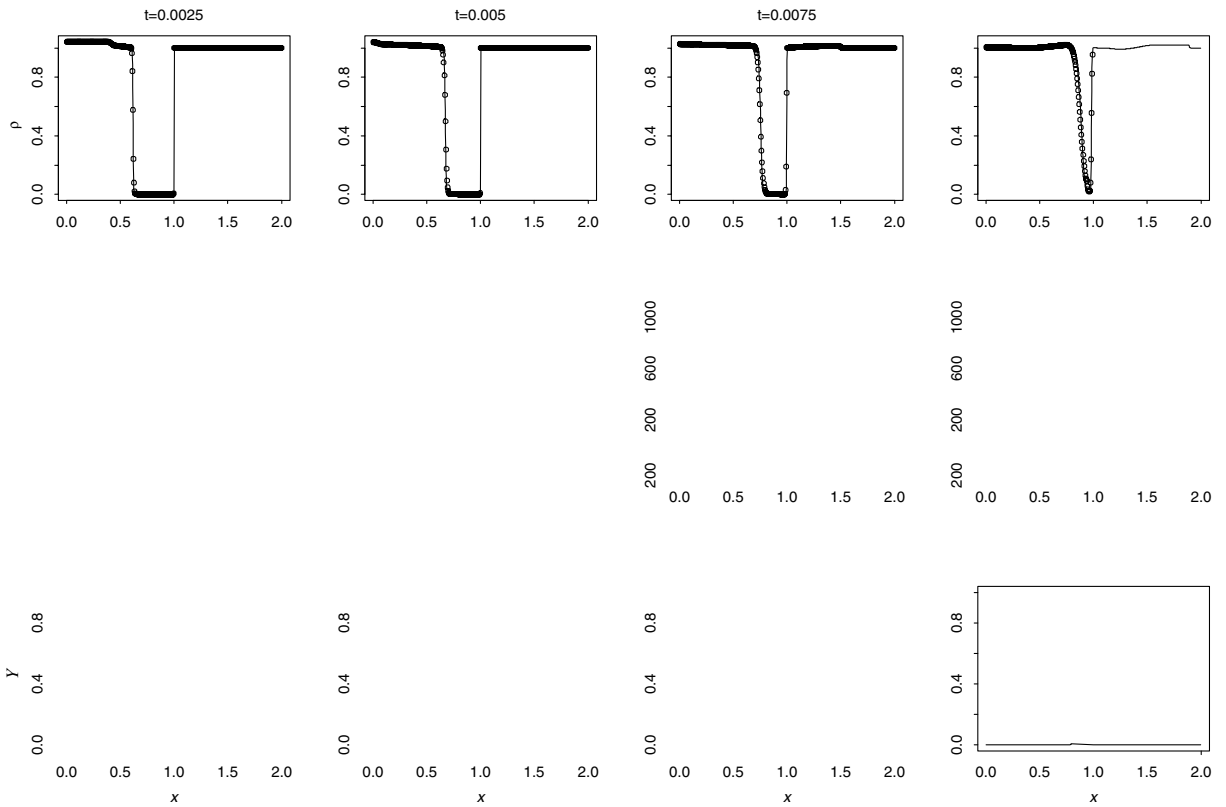

Fig. 9. Cross-sectional plots of the results for the run shown in Fig. 8 along the bottom boundary, where the solid lines are results obtained using the same method but with a finer 800×240 grid.

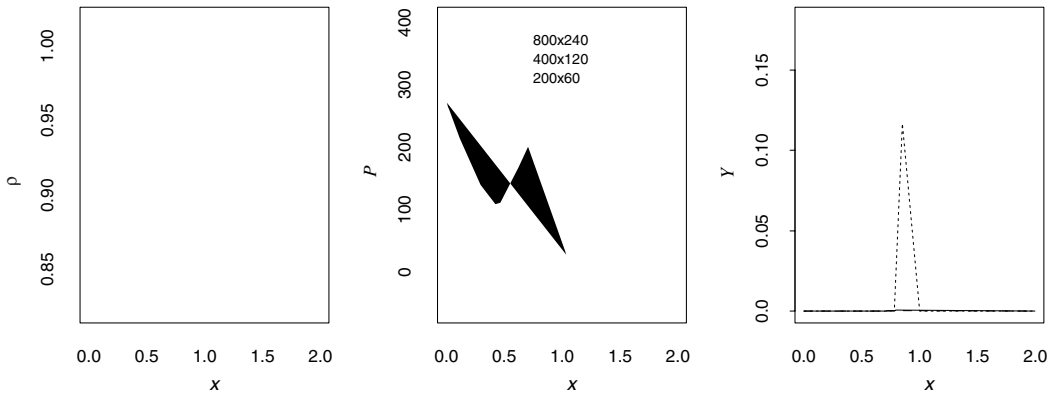

Fig. 10. A convergence study of the y-averaged density, pressure, volume fraction as a function of x for a planar shock wave in water over an air bubble. The test is performed using three different grid systems: $2^i(200 \times 60)$ for $i = 0, 1, 2$, and only the solutions at time $t = 0.01$ is shown.

Example 6.2.4. Finally, we are interested in a shock-contact interaction problem in three space dimensions which may be thought of a continuation of the test performed in Example 6.2.3. Here the problem is set up in the same manner as in the two-dimensional counterpart, with the exception that a shock tube of size

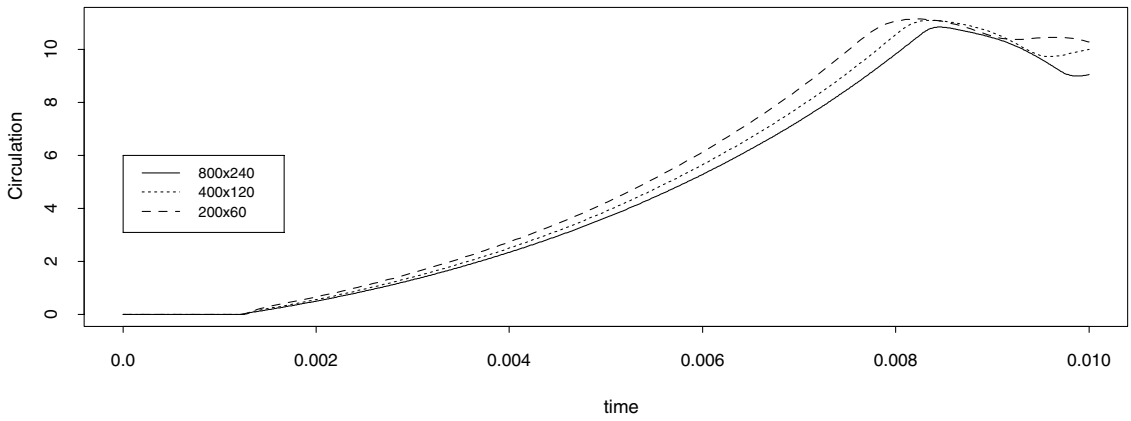

Fig. 11. A convergence study of the total circulation as a function of time for a planar shock wave in water over an air bubble.

$[0,2] \times [0,0.5] \times [0,0.6]$ is used in the computation and the air bubble is now located at $(x_0, y_0, z_0) = (0.8, 0.5, 0)$. Note that the boundary conditions we used in the current case are the non-reflecting boundary condition on the left and right faces, and the solid wall boundary condition on the remaining top, bottom, front, and back faces.

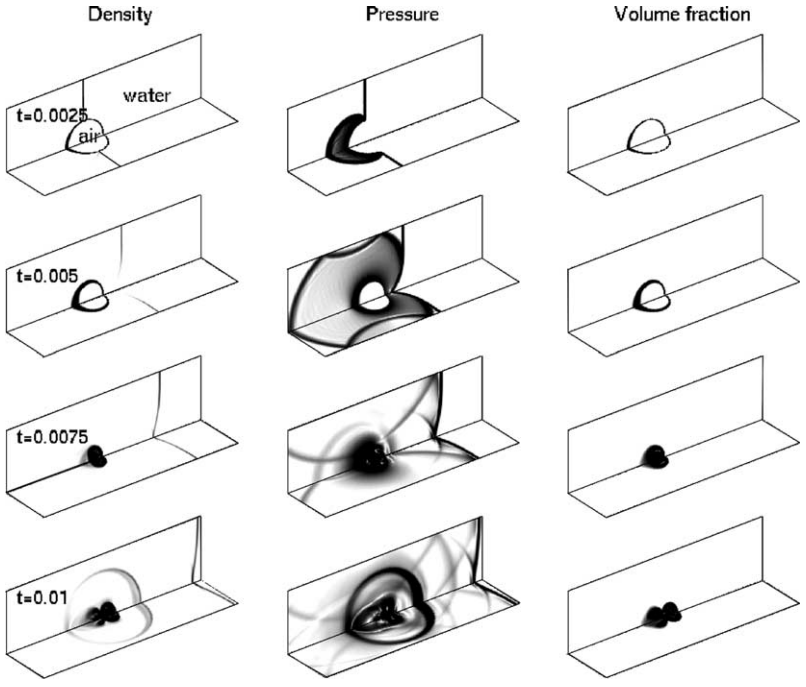

Fig. 12. Three-dimensional results for a planar shock wave in water over an air bubble. Schlieren-type images for the density, pressure, and volume fraction are shown on the planes $y = 0.5$ and $z = 0$ at four different times $t = i \times 0.0025$, for $i = 1, 2, 3, 4$. Here a $400 \times 100 \times 120$ grid was used in the computation.

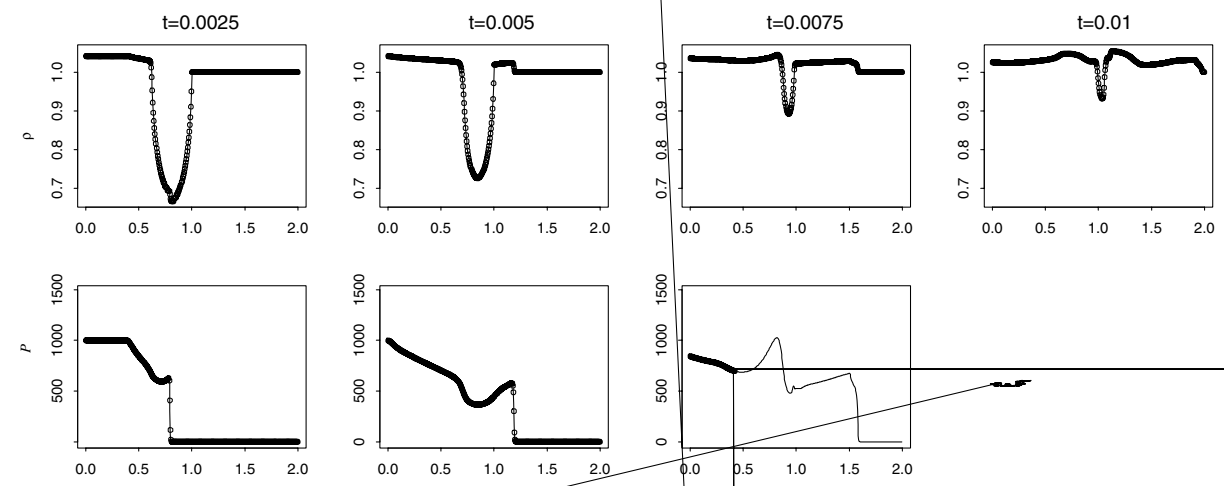

Numerical results of a sample run using a $400 \times 100 \times 120$ grid are shown in Figs. 12 and 13, where in the former a Schlieren-type images of the density, pressure, and volume fraction are plotted on the planes $y = 0.5$ and $z = 0$ at four different times $t = i \times 0.0025$, for $i = 1, 2, 3, 4$, and in the latter a one-dimensional

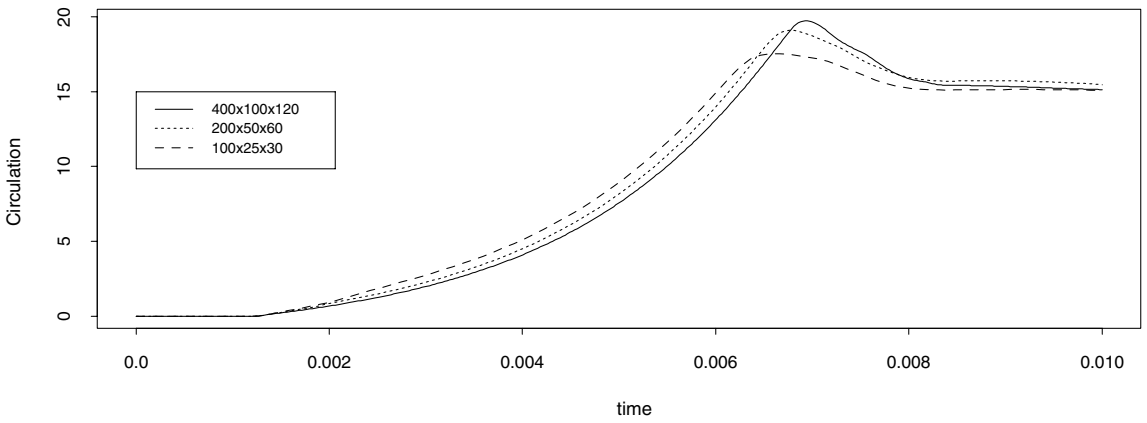

Fig. 15. A convergence study of the circulation around the boundary curve of the $y = 0.5$ plane as a function of time for a three-dimensional case of a planar shock wave in water over an air bubble.

plot of the z-averaged data, defined as $\bar{\zeta}(x) = \sum_{k=1}^{N} \zeta(x, y_M, z_k)/N$, for $\zeta = \rho$, p, or Y, are drawn at the selected times. Here N is the total number of grid cells in the z-direction, and $y_M = 0.5$. Note that, to validate the computed solutions, in Fig. 13 we also include results obtained using the same method but with a finer $500 \times 125 \times 150$ grid, and find good agreement of these two solutions. It is interesting to see that, as far as the global structure of the solution is concerned, from Fig. 12, we observe quite similar results as in comparison with the two-dimensional result presented in Fig. 8.

Here, to investigate the convergence behavior of the algorithm, we perform a mesh refinement study of the solution using the following grid sequence: $2^i(100 \times 25 \times 30)$, for $i = 0, 1, 2$. Fig. 14 shows results of the yz-averaged data, defined as $\widetilde{\zeta}(x) = \sum_{j=1}^{M} \sum_{k=1}^{N} \zeta(x, y_j, z_k)/MN$, for $\zeta = \rho$, p, or Y, at the time $t = 0.01$, where M and N are the total number of grid cells in the y- and z-direction, respectively. From the plot, we notice sensible convergence behavior of the solutions in most part of the domain, without any spurious oscillations in the pressure near the air–water interface. The temporal resolution of the circulation around the boundary curve of the $y = 0.5$ plane is presented in Fig. 15, giving further evidence of the viability of the algorithm to practical barotropic two-fluid problems.

7. Conclusion

We have described a simple interface-capturing approach for barotropic two-fluid flow problems in more than one space dimension. The algorithm uses a non-isentropic form of the equation of state for the modeling of the numerically induced mixing between two different barotropic fluid components within a grid cell. Following the previous work, we devise a mixture-type of the governing equations to ensure a consistent approximation of the energy equation near the smeared time-dependent material interfaces. Note that here the pressure is computed directly from the equation of state as in the single component flow. A standard high-resolution method based on the wave-propagation formulation is employed to solve the proposed model equations with the dimensional-splitting technique included in the method for multidimensional problems. Numerical results presented in this paper demonstrate clearly the feasibility of the approach for a reasonable class of two-fluid problems with the thermodynamic property of each fluid component characterized by the Tait equation of state. In the future, we plan to further extend the algorithm that has the capability of dealing with the effect of the slip condition on the velocity across the in-

terface which will be important for applications such as the propagation of pressure wave in bubbly flow (cf. [19,20,41,49]), and also to cavitating flow problems (cf. [4]).

Acknowledgements

This work was supported in part by National Science Council of Republic of China Grants NSC-90-2115-M-002-022, and 91-2115-M-002-016. The author thanks the anonymous reviewers for the useful comments and English corrections that helped to improve the first draft of the manuscript.

References

[1] R. Abgrall, How to prevent pressure oscillations in multicomponent flow calculations: a quasi conservative approach, J. Comput. Phys. 125 (1996) 150–160.
[2] R. Abgrall, S. Karni, Computations of compressible multifluids, J. Comput. Phys. 169 (2001) 594–623.
[3] G. Allaire, S. Clerc, S. Kokh, A five-equation model for the simulation of interface between compressible fluids, J. Comput. Phys. 181 (2002) 577–616.
[4] T. Barberon, P. Helluy, Finite volume simulation of cavitating flows, Comput. Fluids (2004), to appear.
[5] T. Barberon, P. Helluy, S. Rouy, Practical computation of axisymmetrical multifluid flows, Int. J. Finite Volumes 1 (2003) 1–34.
[6] P. Batten, N. Clarke, C. Lambert, D. Causon, On the choice of wave speeds for the HLLC Riemann solvers, SIAM J. Sci. Comput. 18 (1997) 1553–1570.
[7] P. Colella, Glimm's method for gas dynamics, SIAM J. Sci. Stat. Comput. 3 (1) (1982) 76–110.
[8] P. Colella, H.M. Glaz, Efficient solution algorithms for the Riemann problem for real gases, J. Comput. Phys. 59 (1985) 264–289.
[9] R. Courant, K.O. Friedrichs, Supersonic Flow and Shock waves, Wiley-Interscience, New York, 1948.
[10] S.F. Davis, Simplified second-order Godunov-type methods, SIAM J. Sci. Stat. Comput. 9 (1988) 445–473.
[11] J.R. Edwards, R.K. Franklin, M.-S. Liou, Low-diffusion flux-splitting methods for real fluid flows with phase transition, AIAA J. 38 (2000) 1624–1633.
[12] R.P. Fedkiw, T. Aslam, B. Merriman, S. Osher, A non-oscillatory Eulerian approach to interfaces in multimaterial flows (the ghost fluid method), J. Comput. Phys. 152 (1999) 457–492.
[13] E. Fermi, Thermodynamics, Dover, New York, 1956.
[14] E. Godlewski, P.-A. Raviart, Numerical Approximation of Hyperbolic Systems of Conservation Laws, Applied Mathematical Science, vol. 118, Springer-Verlag, 1996.
[15] R.K.S. Hankin, The Euler equations for multiphase compressible flow in conservation form: Simulation of shock-bubble interactions, J. Comput. Phys. 172 (2001) 808–826.
[16] A. Harten, P.D. Lax, B. van Leer, On upstream differencing and Godunov-type schemes for hyperbolic conservation laws, SIAM Rev. 25 (1983) 35–61.
[17] M.J. Ivings, D.M. Causon, E.F. Toro, On Riemann solvers for compressible liquids, Int J. Numer. Meth Fluids 28 (1998) 395–418.
[18] P. Jenny, B. Mueller, H. Thomann, Correction of conservative Euler solvers for gas mixtures, J. Comput. Phys. 132 (1997) 91–107.
[19] M. Kameda, Y. Matsumoto, Shock waves in a liquid containing small gas bubbles, Phys. Fluids 8 (1996) 322–335.
[20] M. Kameda, N. Shimaura, F. Higashino, Shock waves in a uniform bubbly flow, Phys. Fluids 10 (10) (1998) 2661–2668.
[21] S. Karni, Multicomponent flow calculations by a consistent primitive algorithm, J. Comput. Phys. 112 (1994) 31–43.
[22] D. Kincaid, W. Cheney, Numerical Analysis Brooks/Cole, 1990.
[23] B. Koren, M.R. Lewis, E.H. van Brummelen, B. van Leer, Riemann-problem and level-set approaches for homentropic two-fluid flow computations, J. Comput. Phys. 185 (2002) 654–674.
[24] J.O. Langseth, R.J. LeVeque, A wave propagation method for three-dimensional hyperbolic conservation laws, J. Comput. Phys. 165 (2000) 126–166.
[25] R.J. LeVeque, High resolution finite volume methods on arbitrary grids via wave propagation, J. Comput. Phys. 78 (1988) 36–63.
[26] R.J. LeVeque, Numerical Methods for Conservation Laws, second ed., Birkhäuser-Verlag, 1992.
[27] R.J. LeVeque, Wave propagation algorithms for multi-dimensional hyperbolic systems, J. Comput. Phys. 131 (1997) 327–353.
[28] R.J. LeVeque, Finite Volume Methods for Hyperbolic Problems, Cambridge University Press, 2002.
[29] R.J. LeVeque, K.-M. Shyue, One-dimensional front tracking based on high resolution wave propagation methods, SIAM J. Sci. Comput. 16 (1995) 348–377.

[30] A. Marquina, P. Mulet, A flux-split algorithm applied to conservative models for multicomponent compressible flows, J. Comput. Phys. 185 (2003) 120–138.
[31] S.P. Marsh, LASL Shock Hugoniot Data, University of California Press, Berkeley, 1980.
[32] G.H. Miller, P. Colella, A high-order Eulerian Godunov method for elastic-plastic flow in solids, J. Comput. Phys. 167 (2001) 131–176.
[33] G.H. Miller, E.G. Puckett, A high order Godunov method for multiple condensed phases, J. Comput. Phys. 128 (1996) 134–164.
[34] F.D. Murnaghan, Finite Deformation of an Elastic Solid, Wiley, New York, 1951.
[35] H. Nagoya, T. Obara, K. Takayama, Underwater shock wave propagation and focusing in inhomogeneous media, in: R. Brun, L.Z. Dumitrescu (Eds.), Proceedings of the 19th International Symposium on Shock Waves, Marseille, Springer-Verlag, Berlin, 1995, pp. 439–444.
[36] J.M. Picone, J. Boris, Vorticity generation by shock propagation through bubbles in gas, J. Fluid Mech. 189 (1988) 23–51.
[37] E.G. Puckett, J.S. Saltzman, A 3D adaptive mesh refinement algorithm for multimaterial gas dynamics, Physica D 60 (1992) 84–93.
[38] J.J. Quirk, S. Karni, On the dynamics of a shock-bubble interaction, J. Fluid Mech. 318 (1996) 129–163.
[39] P.L. Roe, Fluctuations, signals- A framework for numerical evolution problems, in: K.W. Morton, M.J. Baines (Eds.), Numerical Methods for Fluid Dynamics, Academic Press, 1982, pp. 219–257.
[40] P.L. Roe, Upwind schemes using various formulations of the Euler equations, in: F. Angrand, A. Dervieux, J.A. Desideri, R. Glowinski (Eds.), Numerical Methods for the Euler Equations of Fluid Dynamics, SIAM, 1985, pp. 14–31.
[41] T. Saito, M. Marumoto, H. Yamashita, S.H.R. Hosseini, A. Nakagawa, T. Hirano, K. Takayama, Experimental and numerical studies of underwater shock wave attenuation, Shock Waves 13 (2003) 139–148.
[42] R. Saurel, R. Abgrall, A multiphase Godunov method for compressible multifluid and multiphase flows, J. Comput. Phys. 150 (1999) 425–467.
[43] R. Saurel, R. Abgrall, A simple method for compressible multifluid flows, SIAM J. Sci. Comput. 21 (1999) 1115–1145.
[44] R. Saurel, P. Cocchi, P.B. Butler, Numerical study of cavitation in the wake of hyperbolic underwater projectile, J. Propulsion and Power 15 (1999) 513–522.
[45] K.-M. Shyue, An efficient shock-capturing algorithm for compressible multicomponent problems, J. Comput. Phys. 142 (1998) 208–242.
[46] K.-M. Shyue, A fluid-mixture type algorithm for compressible multicomponent flow with van der Waals equation of state, J. Comput. Phys. 156 (1999) 43–88.
[47] K.-M. Shyue, A volume-of-fluid type algorithm for compressible two-phase flows, in: Hyperbolic Problems: Theory, Numerics, Applications, International Series of Numerical Mathematics, vol. 130, Birkhäuser-Verlag, 1999, pp. 895–904.
[48] K.-M. Shyue, A fluid-mixture type algorithm for compressible multicomponent flow with Mie-Grueneisen equation of state, J. Comput. Phys. 171 (2001) 678–707.
[49] H.B. Stewart, B. Wendroff, Two-phase flows: models and methods, J. Comput. Phys. 56 (1984) 363–409.
[50] G. Strang, On the construction and comparison of difference schemes, SIAM J. Numer. Anal. 5 (1968) 506–517.
[51] P.K. Sweby, High resolution schemes using flux limiters for hyperbolic conservation laws, SIAM J. Numer Anal. 21 (1984) 995–1011.
[52] E.F. Toro, Riemann Solvers and Numerical Methods for Fluid Dynamics: A Practical Introduction, second ed., Springer-Verlag, 1999.
[53] E.F. Toro, M. Spruce, W. Speares, Restoration of the contact surface in the HLL-Riemann solver, Shock Waves 4 (1994) 25–34.
[54] E.H. van Brummelen, B. Koren, A pressure-invariant conservative Godunov-type method for barotropic two-fluid flows, J. Comput. Phys. 185 (2003) 289–308.
[55] D.R. van der Heul, C. Vuik, P. Wesseling, A staggered scheme for hyperbolic conservation laws applied to unsteady sheet cavitation, Comput. Visual Sci. 2 (1999) 63–68.
[56] F. Xiao, T. Yabe, A method to trace sharp interface of two fluids in calculations involving shocks, Shock Waves 4 (1994) 101–108.
[57] K. Yamada, H. Nagoya, K. Takayama, Shock wave reflection and refraction over a two-fluid interface, in: R. Brun, L.Z. Dumitrescu (Eds.), Proceedings of the 19th International Symposuum on Shock Waves, Marseille, Springer-Verlag, Berlin, 1995, pp. 299–304.
[58] D.L. Youngs, Time-dependent multi-material flow with large fluid distortion, in: K.W. Morton, M.J. Baines (Eds.), Numerical Methods for Fluid Dynamics, Academic Press, 1982, pp. 273–285.
[59] Y.B. Zel'dovich, Y.P. Raizer, in: Physics of Shock Waves and High-Temperature Hydrodynamic Phenomena, vols. I & II, Academic Press, 1967.